Toxicology 512 (2025) 154081

Contents lists available at ScienceDirect

Toxicology

journal homepage: www.elsevier.com/locate/toxicol

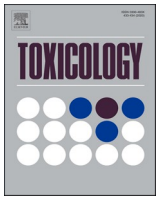

# Hepatic and extra-hepatic metabolism of propylene glycol ethers in the context of central nervous system toxicity

Sophie Werner [a,b,c], David Pamies [c,d], Marie-Gabrielle Zurich [c,d], Laura Suter-Dick [a,c,*]

[a] University of Applied Sciences and Arts Northwestern Switzerland, School of Life Sciences, Muttenz, Switzerland
[b] Department of Pharmaceutical Sciences, University of Basel, Basel, Switzerland
[c] Swiss Centre for Applied Human Toxicology (SCAHT), Basel, Switzerland
[d] Department of Biomedical Science, University of Lausanne, Lausanne, Switzerland

ARTICLE INFO

Handling Editor: Mathieu Vinken

*Keywords:*
Neurotoxicity
Glycol ether
Hepatic metabolism
Extra-hepatic metabolism
blood-brain barrier
*In silico*
Alcohol- and aldehyde dehydrogenase

ABSTRACT

Propylene glycol ethers (PGEs) are mixtures of an α-isomer and a β-isomer (β-PGE) that is oxidized *via* alcohol dehydrogenase (ADH) and aldehyde dehydrogenase (ALDH) to potentially neurotoxic alkoxy propionic acids (β-metabolites). While the liver is the primary organ for ADH- and ALDH-mediated metabolism, the contribution to the metabolism of β-PGEs by the blood-brain barrier (BBB) and the brain remains unknown. Here, we aimed to assess the neurotoxic potential of PGEs after systemic exposure by **(1)** comparing 3D HepaRG and human liver subcellular fraction (S9) for the *in vitro* determination of the kinetics of hepatic metabolism for β-PGEs, **(2)** evaluating the BBB-permeability of PGEs and β-metabolites, **(3)** determining the presence of ADH1 and ALDH2 and the extent of metabolization of β-PGEs in the BBB and brain. The results show that 3D HepaRG and S9 served as competent systems to estimate the enzymatic kinetic (clearance) for β-metabolite formation. We observed that PGEs and the β-metabolites could cross the BBB, based on their permeance across a cellular barrier consisting of the hCMEC/D3 cell line. Metabolic enzymes were not exclusive to the liver, as expression of ADH1 and ALDH2 was demonstrated using RT-qPCR, Western blot, and immunostainings in the BBB *in vitro* models and in BrainSpheres. Furthermore, LC-MS/MS quantification of the β-metabolites in all *in vitro* models revealed that 3D HepaRG had a similar metabolic capacity to primary human hepatocytes and that the amount of β-metabolite formed per protein in the BBB was approximately 10–30 % of that in the liver. We also demonstrated active metabolism in the BrainSpheres. In conclusion, the hepatic *in vitro* models provided data that will help to refine toxicokinetic models and predict internal exposures, thereby supporting the risk assessment of PGEs. In addition, the high permeance of the PGEs and the β-metabolites across the BBB increases the plausibility of neurotoxicity upon systemic exposure. This is further supported by the presence of active ADH1 and ALDH2 enzymes in the BBB *in vitro* systems and in BrainSpheres, suggesting metabolite formation in the central nervous system. Hence, we suggest that BBB-permeance and extra-hepatic metabolism of the β-PGEs may contribute to the neurotoxicity of PGEs.

*Abbreviations:* ADH, alcohol dehydrogenase; ALDH, aldehyde dehydrogenase; AlogP, Ghose-Crippen LogKow; BBB, blood-brain barrier; β-metabolites, alkoxy propionic acids; $CL_h$, hepatic organ clearance; $CL_{int}$, hepatic intrinsic clearance; CNS, central nervous system; EGE, ethylene glycol ether; $fu_{inc}$, incubational binding; $fu_b$ , plasma binding; FPSA-3, fractional charge weighted partial positive surface area/total molecular surface area; GC-MS, gas chromatography mass-spectroscopy; HPLC-MS/MS, high-performance liquid chromatography mass-spectroscopy; IVIVE, *in vitro-in vivo* extrapolation; $K_m$, Michaelis-Menten-Constant; logBPR, predicted brain/plasma ratio; logP, octanol-water partition coefficient; MMK, Michaelis-Menten kinetic; nHBAcc, number of hydrogen bond acceptors; S9, human liver subcellular fraction; β-PGEs, β-isomer of the PGE; PGE, propylene glycol ether; pHH, primary human hepatocytes; pKa, acid dissociation constant; tPSA, topological polar surface area; $V_{max}$, maximum reaction rate.

* Correspondence to: School of Life Sciences, University of Applied Sciences and Arts Northwestern Switzerland, Hofackerstrasse 30, Muttenz 4132, Switzerland.
*E-mail addresses:* sophie.werner@fhnw.ch (S. Werner), david.pamies@unil.ch (D. Pamies), marie-gabrielle.zurichfontanellaz@unil.ch (M.-G. Zurich), laura.suterdick@fhnw.ch (L. Suter-Dick).

https://doi.org/10.1016/j.tox.2025.154081
Received 9 January 2025; Received in revised form 5 February 2025; Accepted 6 February 2025
Available online 8 February 2025

## 1. Introduction

Several neurological disorders have been associated with occupational exposure to organic solvents (Brown et al., 2005; Pearce and Kromhout, 2014). In the past, it has been well described that alkoxy acetic acid metabolites are responsible for the observed adverse effects of some banned ethylene glycol ethers (EGEs). The presumably less toxic replacement solvents, propylene glycol ethers (PGEs), are commonly sold as technical grade mixtures of secondary (α-isomer) and primary (β-isomer, generally < 5 %) alcohols. Similarly to the EGEs, the primary alcohol group of the β-isomer PGEs is enzymatically oxidized by alcohol dehydrogenase (ADH) and aldehyde dehydrogenase (ALDH) to alkoxy propionic acids (β-metabolites) as the major reaction product (Aasmoe et al., 1998; Aasmoe and Aarbakke, 1999; Carney et al., 2003; Miller et al., 1983, 1984; Moslen et al., 1995; Werner et al., 2024). Consequently, although the proportion of β-PGE in commercial PGEs is considered to be low, adverse effects such as neurotoxicity through the formation of β-metabolites cannot be excluded. Several studies indicate that ADH class I (ADH1), consisting of the subunits alpha (ADH1A), beta (ADH1B), and gamma (ADH1C), and ALDH2 play a significant role in the metabolism of glycol ethers (Aasmoe et al., 1998; Aasmoe and Aarbakke, 1999; Crabb et al., 2004; Wang et al., 2020; Wang and He, 2018).

Knowing the localization and extent of β-metabolite formation in the body is important for estimating PGE and β-metabolite brain exposures and thus predicting neurotoxic effects (Benet and Zia-Amirhosseini, 1995; Kanebratt et al., 2021). The liver is well known for its metabolic activity and has been extensively studied regarding ADH- and ALDH-mediated alcohol metabolism (Crabb et al., 2004; Edenberg, 2007; Wang et al., 2020). Nowadays, a variety of *in vitro* liver systems are available for evaluating the hepatic metabolism of compounds, ranging from cheap and easy-to-use cell fractions to more complex and physiological models like 3D liver cultures (Sodhi and Benet, 2021). While primary human hepatocytes are considered the gold standard to assess metabolism and toxicity *in vitro*, we recently demonstrated the successful use of a 3D model prepared from the well-characterized HepaRG cell line (Mandon et al., 2019; Ramaiahgari et al., 2017) to study the hepatic metabolism of β-isomer propylene glycol methyl ether (β-PGME) (Werner et al., 2024).

Although the liver is the main site for the metabolism of alcohols, they can also be metabolized in the central nervous system (CNS), with ADH and CYP2E1 being the main responsible enzymes (Heit et al., 2013). However, limited data exists for ADH1 in the CNS, although it is the main isoform responsible for glycol ether metabolism (Aasmoe et al., 1998; Aasmoe and Aarbakke, 1999; Crabb et al., 2004). Only a few studies have reported its presence on the gene and protein level (Heit et al., 2013; Laniewska-Dunaj et al., 2013; Martínez et al., 2001; Quertemont, 2004). To our knowledge, no studies reporting the activity of ADH1 in the CNS exist, leaving its role in extra-hepatic metabolism of PGEs unknown. In contrast, the presence and activity of mitochondrial ALDH2 in the CNS have been reported, although its role in alcohol metabolism in the brain is not yet fully understood (Chen, 2020; Laniewska-Dunaj et al., 2013; Pervin and Stephen, 2021; Quertemont, 2004). Extra-hepatic metabolism of PGEs within the CNS, alongside hepatic metabolism, could enhance the potential neurotoxicity caused by their β-metabolites. This would be particularly relevant for exposure routes avoiding first-pass metabolism through the liver, such as inhalation.

For PGEs to exert effects on the CNS, they must first cross the blood-brain barrier (BBB), a process influenced by their physicochemical properties (Geldenhuys et al., 2015). A previously reported *in vitro* study already demonstrated high passive BBB permeation for three selected glycol ethers (Reale et al., 2023). However, BBB permeability data is still not available for most PGEs. Here, we implemented the hCMEC/D3 cell line as a well-characterized BBB *in vitro* model frequently used to evaluate the passive permeability coefficient ($P_{app}$) of compounds. It represents a good, accessible and standardized alternative to the primary human brain microvascular endothelial cells (HBMVEC) derived from tissue (Poller et al., 2008; Weksler et al., 2013). The BBB permeance of compounds can also be studied using *in silico* tools such as the online CDK toolkit (Bendels et al., 2008; Suenderhauf et al., 2012a) or admetSAR (Yang et al., 2019). They are inexpensive and high-throughput screening tools, typically based on the molecular determinants of the compounds (Bagchi et al., 2019; Geldenhuys et al., 2015). Furthermore, substances that compromise BBB integrity would allow the entry into the CNS of molecules normally excluded, potentially leading to indirect neurotoxicity (Haorah et al., 2005; Wei et al., 2021). Consequently, it is also crucial to evaluate the toxicity of the PGEs to the BBB.

Neurotoxic effects on the brain can be investigated in animal models or by implementing human-relevant systems (Price et al., 2018). Here, we performed studies on the recently developed 3D human induced pluripotent stem cells (hiPSC)-derived brain model (BrainSpheres) (Pamies et al., 2017). This model contains several subtypes of neurons, astrocytes, and oligodendrocytes, and has already proven its utility for neurotoxicity testing (Nunes et al., 2023; Pamies et al., 2021, 2018).

Few PGEs have been studied for neurological effects; CNS depression was reported at high doses in rodents (Landry and Yano, 1984; Miller et al., 1984), but no long-term neurotoxicity has been observed. To date, studies on the neurotoxicity of PGEs and their β-metabolites after systemic exposure are rare and limited data exists (ECETOC, 2005a, 2005b). To address this gap, Hopf et al. (2024) proposed a novel strategy for assessing the neurotoxicity of several PGEs by combining *in vitro* and *in silico* methods with human-controlled exposure studies. Our study contributes to this approach by generating new *in vitro* hepatic kinetic data for selected β-isomers of PGEs and assessing the potential of PGEs to cross and/or damage the BBB and produce β-metabolites within the CNS. To this end, we determined *in vitro* hepatic intrinsic clearance ($CL_{int}$) of subtoxic concentrations of β-PGEs using an established 3D HepaRG model and human liver subcellular fraction (S9). Subsequently, we evaluated the *in vitro* $P_{app}$ for the PGEs and their β-metabolites, as well as for ethylene glycol methyl ether (EGME) as a comparator, in the hCMEC/D3 BBB *in vitro* model and compared the results to *in silico* permeability predictions and the physicochemical properties of the substances. Finally, we demonstrated the expression of the two enzymes ADH1 and ALDH2 and the formation of the β-metabolites in the BBB models (hCMEC/D3, HBMVEC) and BrainSpheres, demonstrating hepatic and extra-hepatic metabolism of PGEs.

## 2. Material and methods

### 2.1. Chemicals and S9 fractions

1-Butoxypropan-2-ol (PGBE, > 99 %), 2-Butoxypropionic acid (2-BPA, > 95 %), 1-Ethoxypropan-2-ol (PGEE, > 95 %), 2-Ethoxypropan-1-ol (β-PGEE, > 95 %), 2-Ethoxypropionic acid (2-EPA), 2-Methoxyacetic acid (2-MAA, 98 %), 2-Methoxyethanol (EGME, 99.8 %), 1-Methoxypropan-2-ol (PGME, > 99.5 %), 2-Methoxypropionic acid (2-MPA, > 97 %), 1-Phenoxypropan-2-ol (PGPhE, > 93 %), 2-Phenoxypropan-1-ol (β-PGPhE, > 95 %), 2-Phenoxypropionic acid (2-PhPA, > 98 %), 1-Propoxypropan-2-ol (PGPE, 99 %), and 2-Propoxypropionic acid (2-PPA, 95 %) were purchased from Sigma-Aldrich (St. Louis, MO, USA). 2-Methoxypropan-1-ol (β-PGME, 98 %) was manufactured by aa blocks (San Diego, CA, USA). Glycol ethers and the alkoxy acids (β-metabolites) are listed in Table 1 and Fig. 1. Ultrapure water was obtained from a Millipore Milli-Q Plus purification system (Bedford, MA, USA). Phosphate buffer was prepared in-house, adjusted to pH 7.4, and stored at 4 °C. All other chemicals and reagents were of analytical grade and purchased from commercial sources, except 2-Butoxypropan-1-ol (β-PGBE) that was synthesized in-house due to commercial non-availability (analytical grade > 99 %, Supplementary Figs. 1–3). Pooled adult mixed gender human liver subcellular fraction (S9) was purchased from

**Table 1**
Overview of the glycol ethers and β-metabolites and the analyzed data.

| CAS number | IUPAC Name | Trivial name | Abbreviation | Molecular Weight (MW)[a] | LogP[a] | pKa[b] | $fu_{,b}$[c] | Cytotoxicity study 3D HepaRG & hCMEC/D3 | Hepatic clearance study | Permeability study hCMEC/D3 | Metabolite formation study |
|---|---|---|---|---|---|---|---|---|---|---|---|
| 109-86-4 | 2-Methoxyethanol | Ethylene glycol methyl ether | EGME | 76.09 | - 0.80 | 15.10 (A) | ND | (Werner et al., 2024) | ND | Yes | ND |
| 107-98-2 | 1-Methoxypropan-2-ol | Propylene glycol methyl ether | PGME | 90.12 | - 0.49 | 14.85 (A) | ND | (Werner et al., 2024) | ND | Yes | ND |
| 1589-47-5 | 2-Methoxypropan-1-ol | | β-PGME | 90.12 | - 0.49 | 14.69 (A) | ND | (Werner et al., 2024) | (Werner et al., 2024) | Yes | 3D HepaRG, 3D pHH, hCMEC/D3, HBMVEC |
| 1569-02-4 | 1-Ethoxypropan-2-ol | Propylene glycol ethyl ether | PGEE | 104.2 | 0.30 | 14.85 (A) | 0.688 | Yes | ND | Yes | ND |
| 19089-47-5 | 2-Ethoxypropan-1-ol | | β-PGEE | 104.2 | 0.20* | 14.69 (A) | 0.710 | Yes | 3D HepaRG[e] | Yes | 3D HepaRG, 3D pHH, hCMEC/D3, HBMVEC |
| 1569-01-3 | 1-Propoxypropan-2-ol | Propylene glycol propyl ether | PGPE | 118.2 | 0.70 | 14.85 (A) | ND | Yes | ND | Yes | ND |
| 10215-30-2 | 2-Propoxypropan-1-ol | | β-PGPE[d] | 118.2 | 0.70 | 14.69 (A) | ND | - | - | - | - |
| 5131-66-8 | 1-Butoxypropan-2-ol | Propylene glycol butyl ether | PGBE | 132.2 | 1.15 | 14.85 (A) | 0.478 | Yes | - | Yes | - |
| 15821-83-7 | 2-Butoxypropan-1-ol | | β-PGBE | 132.2 | 1.10* | 14.69 (A) | 0.491 | Yes | S9, 3D HepaRG | No | 3D HepaRG, 3D pHH, < LOD for BBB models |
| 770-35-4 | 1-Phenoxypropan-2-ol | Propylene glycol phenyl ether | PGPhE | 152.2 | 1.50 | 14.83 (A) | 0.390 | Yes | - | Yes | - |
| 4169-04-4 | 2-Phenoxypropan-1-ol | | β-PGPhE | 152.2 | 1.60* | 14.67 (A) | 0.366 | Yes | S9, 3D HepaRG | Yes | 3D HepaRG, 3D pHH, < LOD for BBB models |
| 625-45-6 | 2-Methoxyacetic acid | Methoxy acetic acid | 2-MAA | 90.08 | - 0.30 | 3.83 (A) | ND | (Werner et al., 2024) | - | Yes | - |
| 4324-37-2 | 2-Methoxypropionic acid | Methoxy propionic acid | 2-MPA | 104.1 | 0.10* | 3.99 (A) | ND | (Werner et al., 2024) | - | Yes | - |
| 53103-75-6 | 2-Ethoxypropionic acid | Ethoxy propionic acid | 2-EPA | 118.1 | 0.40* | 4.14 (A) | ND | Yes | - | Yes | - |
| 56674-67-0 | 2-Propoxypropionic acid | Propoxy propionic acid | 2-PPA | 132.2 | 1.00 | 4.35 (A) | ND | Yes | - | Yes | - |
| 14620-87-2 | 2-Butoxypropionic acid | Butoxy propionic acid | 2-BPA | 146.2 | 1.30* | 4.35 (A) | ND | Yes | - | Yes | - |
| 940-31-8 | 2-Phenoxypropionic acid | Phenoxy propionic acid | 2-PhPA | 166.2 | 1.70* | 3.78 (A) | ND | Yes | - | Yes | - |

ND: not determined.
Abbreviations: logP: octanol-water partition coefficient; pKa: acid dissociation constant, with (A) for acid; $fu_{,b}$: plasma binding; pHH: primary human hepatocytes; HBMVEC: human brain microvascular endothelial cells; LOD: limit of detection; BBB: blood-brain barrier.
[a] Data retrieved January 12, 2024, from Pubchem. PubChem (nih.gov).
[b] Data retrieved January 12, 2024, from Chemicalize. Chemicalize - Instant Cheminformatics Solutions.
[c] Data retrieved January 12, 2024, from QIVIVE, https://www.qivivetools.wur.nl.
[d] Compound not available.
[e] S9 data will be published elsewhere.
* Computed data.

Thermosphere Scientific (Reinach, Switzerland; HMS9PL) and stored at – 80 °C after aliquoting. Detailed donor information for the S9 lots is summarized in Supplementary Table 1.

### 2.2. Cell culture

The HepaRG cell line was procured from Biopredic International (Saint Grégoire, France; HPR101) and cultured for four weeks in basal medium with growth supplements (Biopredic International; ADD710). The cells were passaged (until passage 20) using Trypsin-EDTA (Sigma, Taufkirchen, Germany; 59417C-100mL). Cell differentiation over two weeks was induced using medium containing a 50:50 mixture of growth and differentiation supplements (Biopredic International; ADD720) for four days, following the use of medium containing solely differentiation supplements for additional 10 days. For cell aggregation, William's E Medium + GlutaMAX (ThermoFisher Scientific; 32551087), 1 × ITS (Sigma; 11074547001), 100 nM Dexamethasone (Sigma; D1756), 1 % penicillin and streptomycin (P/S; Sigma; P4333-100mL), and 20 % fetal bovine serum (FBS; ThermoFisher Scientific; 10270-106) was used. Medium was exchanged for serum-free supplemented William's E Medium at day 5 after aggregation for all treatment conditions.

Cryopreserved primary human hepatocytes (pHH) were obtained from Lonza (Basel, Switzerland; HUCPI). Detailed donor information for the hepatocyte lots is summarized in Supplementary Table 2. Cells were carefully thawed and resuspended in thawing medium (Lonza; MCHT50) before being seeded in fresh plating medium (Lonza; MP100/

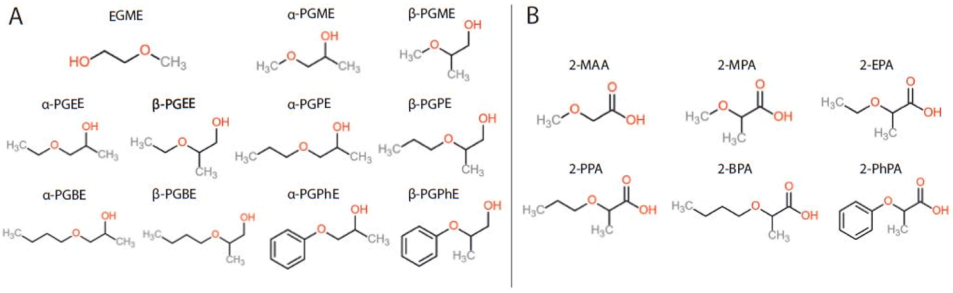


**Fig. 1.** Chemical structures for the studied (A) glycol ethers and (B) alkoxy acid metabolites.

MP250) or aggregation medium for either plated use or 3D culturing, respectively. Plates used for 2D cell culture were coated 1 h before seeding with rat tail collagen type I (1.3 μg/cm$^2$, Sigma; 08-115) and the medium was exchanged daily with maintenance medium (Lonza; CC-3198). The same cell aggregation and treatment media for the 3D cultures were used as described previously for the HepaRG.

Immortalized human brain capillary endothelial cells (hCMEC/D3; Sigma, SCC066) were grown in precoated flasks or plates using rat tail collagen type I (1.3 μg/cm$^2$, Sigma) 1 h prior seeding. EBM-2 medium (Lonza; CC-3156) supplemented with the SingleQuots™ growth factors (Lonza; CC-4176), excluding vascular endothelial growth factor VEGF as recommended by the manufacturer, was used for culturing and treatment. Passaging at 80–90 % confluency was done using Accumax (ThermoFisher Scientific; 00-4666-56) and cells were used at passages 10-22.

Primary human brain microvascular endothelial cells (HBMVEC; ACBRI376) were obtained from Cell Systems (Kirkland, WA, USA). Precoating was performed using the Attachment Factor™ (Cell Systems; 4Z0-201). Cells were carefully thawed using CultureBoost™ (Cell Systems; 4CB-500) and cultured in complete classic medium with serum and CultureBoost™ (Cell Systems; 4Z0-500) for the passages 3–7. Passaging at 80–90 % confluency was performed using the Passage reagent Group™ 1–3 (Cell Systems; 4Z0-800).

Neural progenitor cells (NPCs, GEO-1) were generated from induced pluripotent stem cells (iPSCs) derived from human CCD-1079Sk fibroblasts (ATCC®, Manassas, VA, USA; CRL-2097), as previously described (Hogberg et al., 2013; Wen et al., 2015). NPCs were then grown and amplified in cell culture flasks coated with Geltrex® (ThermoFisher Scientific; A1413201) using Neural Expansion Medium (NEM) consisting of 45 % Neurobasal® Medium (21103049), 45 % Advanced™ DMEM/F-12 Medium (12634010), and 10 % Neuronal Induction Supplement (A1647701), all from ThermoFisher Scientific. The medium was replaced every two to three days. At 90 % confluency, cells were passaged using StemPro™ Accutase™ Cell Dissociation Reagent (ThermoFisher Scientific; A1110501).

BrainSpheres were differentiated from NPCs following published protocols (Pamies et al., 2017). Briefly, NPCs a grown to 95 % confluency were washed with Dulbecco's Phosphate-Buffered Saline (DPBS; Sigma; D8537). StemPro™ Accutase™ Cell Dissociation Reagent was used to detach the cells from the flask. Cells were seeded at 2 × 10$^6$ cells in 2 mL per well in a non-treated six-well plate (Sigma; CLS3516). After two days, the medium was changed to Neuronal Differentiation Medium (NDM), consisting of Neurobasal Electro Medium (A1413701), 2 % B27 Neurobasal Electro supplement (A1413701), 0.01 μg/mL human/-murine/rat recombinant brain-derived neurotrophic factor (BDNF; 450-02-1), 0.01 μg/mL human recombinant glial cell-derived neurotrophic factor (GDNF; 450-10-1), and 100 U/mL penicillin-100 μg/mL streptomycin, all from ThermoFisher Scientific. The medium was replaced three times a week.

All cells were cultured at 37 °C with 5 % $CO_2$ in a 95 % humified incubator, with constant gyratory shaking (Kuhner orbital plate shaker ES-X, 88 rpm) applied for the BrainSpheres.

### 2.3. Cell viability assay

For 2D cultures, HepaRG cells were seeded 7 days prior exposure at 2.25 × 10$^5$ cells/cm$^2$ in a 96-well plate (Corning, NY, USA; 353072). For 3D cultures, HepaRG cells were seeded 7 days prior exposure at 3000 cells per well to form 3D-spheroids in Nunclon™ Sphera™ 96-well U-shaped-bottom microplates (ThermoFisher Scientific; 174925). hCMEC/D3 and HBMVEC were seeded 7 days prior treatment in 96-well plates at 2.34 × 10$^4$ cells/cm$^2$. The acidic pH condition resulting from the β-metabolites in the highest treatment condition (Supplementary Fig. 4) was neutralized to pH 7.4 (measured with an electrode) using 1 N NaOH and sterilized by filtration before further diluted. For the 3D HepaRG cultures, half of the medium was removed, and twofold concentrated compound solution was added. The cell plates were sealed with an adhesive gas permeable seal (ThermoFisher Scientific; AB0718) to prevent solvent evaporation. Compound concentrations in the range of 0.1–1000 mM for the glycol ethers and 0.6–25 mM for the β-metabolites for evaluating concentration-dependent cytotoxicity for single (48 h) or repeated (7 days) exposure were selected, considering solubility limitations of the compounds. Cell viability was assessed subsequently after the incubation period by measuring ATP content using the CellTiter-Glo Luminescent Cell Viability Assay (Promega, USA; G7570) at 48 h and 7 days after exposure, following the manufacturer's instructions. Luminescence was measured on a Flexstation 3 microplate reader (Molecular Devices) at 1000 ms. Following, the $EC_{50}$ was calculated using GraphPad Prism.

### 2.4. Gene expression analysis

HepaRG cells and pHH were seeded at 2.25 × 10$^5$ cells/cm$^2$, and hCMEC/D3 and HBMVEC were seeded at 2.34 × 10$^4$ cells/cm$^2$, in 96-well plates and cultured for 7 days. The total RNA was isolated using the Qiazol Lysis Reagent (Qiagen, Basel, Switzerland; LT-02241) and mRNA isolated following the standard TRIzol extraction procedure with glycogen (ThermoFisher Scientific; 79306). Reverse transcription was performed using the M-MLV Reverse transcriptase (Promega, Dübendorf, Switzerland; M1705) and oligo(dT) (Qiagen; 79237). Quantitative real-time PCR was conducted with specific TaqMan probes for selected genes (see Table 2) and FastStart TaqMan® Probe Master (Sigma; 4673417001). The q-RT-PCR program was following: 10 min denaturation at 95 °C, followed by 40 cycles of 15 s at 95 °C and 1 min at 60 °C. The Ct values were produced using the LightCycler® 480II Systems

**Table 2**
Taqman probes of selected genes obtained from ThermoFisher Scientific.

| Gene of interest | Abbreviation | Ref. nr. |
|---|---|---|
| Alcohol dehydrogenase isoform 1A | ADH1A | Hs00605167_g1 |
| Alcohol dehydrogenase isoform 1B | ADH1B | Hs00605175_m1 |
| Alcohol dehydrogenase isoform 1C | ADH1C | Hs02383872_s1 |
| Aldehyde dehydrogenase 2 | ALDH2 | Hs01007998_m1 |
| Beta-2-Microglobulin | B2M | Hs00187842_m1 |

(Roche Diagnostics, Rotkreuz, Switzerland).

Total RNA was extracted from BrainSpheres automatically (QIAcube instrument, Qiagen) using QIAshredder columns (Qiagen; 79656) and the RNeasy® Mini Kit (Qiagen; 74104). RNA was quantified with NanoDrop™ One Microvolume UV-Vis Spectrophotometer (ThermoFisher Scientific). Reverse transcription was performed using 2 µg of total RNA with the High-Capacity cDNA Reverse Transcription Kit with RNase Inhibitor (ThermoFisher Scientific; 4368814). Real-time PCR was then conducted using Taqman™ Universal PCR Master Mix (ThermoFisher Scientific; 4304437) with specific TaqMan probes for selected genes (see Table 2).

Beta-2-Microglobulin (B2M) was used as internal standard for normalization and relative gene expression was calculated as ΔCt = Ct of the Gene of Interest - Ct B2M.

### 2.5. Immunohistochemistry

hCMEC/D3 and HBMVEC were fixed with 4 % PFA (Polysciences, Warrington, PA; USA; 18814-10) for 15 min and washed in 1 × PBS (Sigma; 11666789001). Cells were permeabilized with 0.1 % Triton X-100 in 1 × PBS (ROTH, Arlesheim, Switzerland; 3051.3) for 15 min, washed and blocked with 1 % BSA in 1 × PBS (Sigma; A2153) for 1 h. After washing again, the primary antibody was incubated overnight (4 °C), washed, followed by the incubation with the secondary antibody (1:1000) for 1 h. Washed cells were counterstained with DAPI (ThermoFisher Scientific; 62248, 1:1000) (2–5 min) prior to imaging. Antibodies and the applied dilutions in 0.1 % BSA in 1 × PBS are listed below (Table 3). The images were taken with the Olympus Fluoview FV3000 Confocal Microscope.

BrainSpheres were fixed for 1 h with 4 % PFA and washed three times with 1 × PBS for 10 min each. Then, they were blocked with 4 % Triton X in 1 × PBS containing 5 % normal goat serum (NGS; ThermoFisher Scientific; 50062Z) for 2 h on a shaker at RT. Afterwards, BrainSpheres were incubated with primary antibodies diluted in 1 × PBS containing 5 % NGS and 1 % Triton X (4 °C, 24 h). Subsequently, BrainSpheres were washed three times and incubated for 2 h at 4 °C with secondary antibodies (1:200) diluted in 1 × PBS containing 5 % NGS. They were then washed three times. Nuclei were stained with Hoechst 33342 trihydrochloride trihydrate (Invitrogen; H3570, 1:10,000) for 10 min at - 4 °C. Finally, BrainSpheres were mounted on glass slides using a mounting medium (ThermoFisher Scientific; P36930). The images were captured using a confocal microscope (Zeiss LSM 780 GaAsP) and visualized using ZEN Imaging software from Zeiss and ImageJ.

**Table 3**
Antibodies used for immunohistochemistry obtained from ThermoFisher Scientific.

| Protein of interest | Abbreviation | Primary antibody | Secondary antibody |
|---|---|---|---|
| Alcohol dehydrogenase 1 | ADH1A/B/C | Goat polyclonal antibody (PAB6725)/1:500 | Rabbit anti-goat Alexafluor 488 (A-11078) |
| Aldehyde dehydrogenase 2 | ALDH2 | Mouse monoclonal antibody (MA5-17029)/ 1:500 | Rabbit anti-mouse Alexafluor 546 (A-11060) |
| CD31 | | Rabbit polyclonal antibody (ab32457)/ 1:1000 | Rabbit anti-goat Alexafluor 488 (A-11078) |
| Phalloidin | | Phalloidin Alexafluor 488 (A12379)/1:100 | - |
| ZO-1 | | Mouse monoclonal antibody (33-9100)/1:100 | Rabbit anti-mouse Alexafluor 546 (A-11060) |

### 2.6. Western blot

Samples of hCMEC/D3, HBMVEC, and BrainSpheres cell lysates were run on a 10 % SDS-Page and transferred to a PVDF membrane (Sigma; GE1060004) using the Pierce Powerplot cassette and power station (ThermoFisher Scientific). Protein concentrations were measured according to the standard Bradford assay protocol using ROTI® Nanoquant (ROTH; K880.1) and the Pierce BCA Protein assay kit (ThermoFisher Scientific, 23225) according to the manufacturer's instructions. Membranes were blocked for 1.5 h with 4 % milk in TBS-T (0.1 % Tween-20) and incubated overnight with the primary antibody at 4 °C. Subsequently, membranes were washed with TBS-T and the secondary antibody was applied for 1 h at RT. All antibodies were diluted in 3 % milk in TBS-T and are listed in Table 4. Imaging was performed using the Odyssey®CLx imaging system (LI-COR Biosciences, Bad Homburg, Germany). The relative signal mean intensity was calculated using ImageJ by measuring the area of bands of interest and normalization to the area of GAPDH.

### 2.7. Evaluation of Michaelis-Menten-kinetics, substrate depletion, and β-metabolite formation using S9 fraction

The incubation mixtures contained S9 (1 mg/mL), 100 mM potassium phosphate buffer (pH 7.4), 3 mM $MgCl_2$, 1 mM $NAD^+$ (Sigma; NAD100-RO), 1 mM NADPH (Sigma; NADPH-RO), and the respective substrate concentrations. A concentration range of 0.1–4.2 mM β-PGPhE or β-PGBE was used for the Michaelis-Menten kinetic (MMK) measurements. For the substrate depletion/β-metabolite formation measurements, the applied substrate concentration was approximately twofold below (90 µM β-PGPhE) or marginally above (140 µM β-PGBE) the determined $K_m$ value. After 5 min of preincubation, the reaction was initiated with the addition of $NAD^+$ and NADPH, and incubations conducted (45 min, 300 rpm, 37 °C) on a Thermomixer (Eppendorf, Hamburg, Germany). Incubations without $NAD^+$ and NADPH were included as a control. Reactions were stopped by the addition of ice-cold acetonitrile (ACN; Sigma; 439134) at 45 min or defined time points over 45 min (1', 12', 23', 34', 45') for the MMK incubations. Samples were then vortexed and centrifuged (15 min, 2500 × *g*, 4 °C) and the supernatant stored at – 80 °C for further analysis. MMK parameters ($V_{max}$ and $K_m$) were obtained by nonlinear regression using GraphPad Prism applying the Michaelis-Menten equation. The *in vitro* hepatic intrinsic clearance ($CL_{int}$) was calculated according to the equations described in Section 2.13.

**Table 4**
Antibodies used for Western blot.

| Protein of Interest | Abbreviation | Primary antibody | Secondary antibody |
|---|---|---|---|
| Alcohol dehydrogenase 1 | ADH1A/B/C | Goat polyclonal antibody (ThermoFisher Scientific; PAB6725)/1:1000 | Donkey anti-goat IRDye® 800CW (LI-COR Biosciences; 925-32214)/1:20,000 |
| Aldehyde dehydrogenase 2 | ALDH2 | Mouse monoclonal antibody (ThermoFisher Scientific; MA5-17029)/1:2000 | Donkey anti-mouse IRDye® 800CW (LI-COR Biosciences; 926-32212)/1:20,000 |
| Glyceraldehyde-3-Phosphate Dehydrogenase | GAPDH | Rabbit polyclonal antibody (ThermoFisher Scientific; PA1-987)/1:1000 | Donkey anti-rabbit IRDye® 680CW (LI-COR Biosciences; 926-68073)/1:20,000 |

### 2.8. Assessment of β-metabolite formation in the different cell systems

For the *in vitro* liver systems, 3D HepaRG and 3D pHH were seeded 7 days before treatment into 96-well ultra-low attachment Elplasia® plates (Corning; 4442) with 219,000 cells per well to form 79 3D-spheroids in micro-arrays (2772 cells/spheroid) per incubation, following centrifugation (2 min, 300 × *g*). For the *in vitro* BBB models, hCMEC/D3 and HBMVEC were seeded 7 days prior treatment in 96-well plates at $2.34 \times 10^4$ cells/cm$^2$. For the 3D HepaRG and pHH, 100 μL medium was removed and 50 μL of threefold concentrated compound solution was added to the remaining 100 μL in the well to reach the final nominal solvent concentration. For the 2D cultures, the medium was replaced by the treatment solution in the final concentration. Non-toxic concentrations of β-PGBE (0.1 mM), β-PGEE (1 mM), and β-PGPhE (0.12 mM), slightly below or at the determined $K_m$ (Table 6, unpublished data for β-PGEE) were used to compare β-metabolite formation under non-saturated conditions. As the experimental set-up required a high nominal concentration of the β-PGEs to meet the limit of quantification for the formed β-metabolites, the applied substrate concentrations were higher than for the S9 incubations. At defined time-points (1 h, 6 h, 24 h), the supernatant was collected, quenched with ice-cold ACN, and stored at – 80 °C for further analysis. 3D HepaRG were lysed at 24 h to perform gene expression analysis as described in Section 2.4. Additionally, supernatant from the 3D HepaRG incubations were collected within the first hour (1', 15', 30', 45') to determine hepatic kinetics and to calculate *in vitro* $CL_{int}$ according to the equations described in Section 2.13. The *in vitro* $CL_{int}$ within the first hour was not determined for the hCMEC/D3 due to the limit of detection.

In addition, BrainSpheres (70–80 per well) were exposed to non-cytotoxic concentrations (20 mM) of β-PGME and β-PGEE, considering full enzyme saturation based on the determined $K_m$ values. Supernatant was sampled after 6 h of incubation and stored at - 80 °C for further analysis.

All incubations were performed in triplicates at 37 °C, 5 % $CO_2$ in a humidified incubator, with constant gyratory shaking (Kuhner orbital plate shaker, 88 rpm) applied for the BrainSpheres, and the plates were covered with a gas permeable seal (except for the BrainSpheres). Before analysis, samples were centrifuged (20 min, 2500 × *g*, 4 °C).

For comparing the β-metabolite generation within the different systems, we normalized the amount of β-metabolite measured (pmol) to the protein amount present per incubation (μg) for each biological replicate (Supplementary Table 3). Determination of protein content per incubation was performed using the Pierce BCA Protein assay kit (ThermoFisher Scientific; 23225) according to the manufacturer's instructions. For comparison of hepatic and extra-hepatic metabolism, the amount of β-metabolite formed normalized per protein for the 3D HepaRG was set as benchmark standard (ratio 1.0) and the relative ratios for the other cell models were calculated. Except for BrainSpheres, for which the experiments were performed under highly saturated conditions.

### 2.9. Evaluation of blood-brain barrier tightness

hCMEC/D3 were seeded at $3 \times 10^3$ cells/cm$^2$ in pre-coated 24-transwells with 0.4 μm polyethylenterephthalate (PET) membrane inserts (cellQART, Northeim, Germany; 9320414) and cultured for 7 days. Subsequently, the cells were incubated for 48 h with the glycol ethers (2 mM) and the β-metabolites (0.1 mM) in a humidified incubator (37 °C, 5 % $CO_2$), placed on an orbital shaker (100 rpm; Eppendorf; New Brunswick S41i). The exposure concentration (2 mM) was selected based on toxicokinetic simulations that predicted a total extravascular concentration exposing the brain of approximately 2 mM with the assumptions: 100 ppm PGME exposure (Swiss occupational exposure limit), 8 h per day, 5 days a week, 100 W workload (N. Hopf, personal communication). An exposure concentration of 0.1 mM for the β-metabolites was selected, accounting for a 5 % *in vitro* β-metabolite formation considering the results from our previously published study (Werner et al., 2024). After 2 h of incubation, supernatant was collected and stored at – 80 °C for further analysis to determine the passive permeability coefficient (see Section 2.10). The tightness of the hCMEC/D3 monolayer was determined by measuring the permeability of the fluorescence marker Lucifer yellow CH dipotassium salt (LY; Sigma; L0144). After 48 h treatment, the medium was removed, 100 μL of 10 μg/mL LY solution was added to the apical compartment and the plate was placed again on the orbital shaker (100 rpm, 1 h) in the incubator. Thereafter, fluorescence (428 nm excitation/540 nm emission) for samples collected from the basolateral chamber was read with a FlexStation 3 microplate reader (Molecular Devices, LCC). LY concentrations were measured applying a standard curve and the apparent permeability ($P_{app}$) was calculated according to Eq. (1):

$$P_{app} \quad [\mathrm{cm/min}] = \frac{V_B \quad [cm^3]}{A \quad [cm^2] \times C_{A0} \quad [\mu L]} \quad \times \quad \frac{\Delta C_B \quad [\mu g/mL]}{\Delta T \quad [\mathrm{min}]} \qquad (1)$$

where $V_B$ is the volume in the basolateral compartment (0.6 cm$^3$), A is the surface area of the filter (0.33 cm$^2$), $C_{AO}$ is the initial concentration in the apical chamber, and $\Delta C_B/\Delta T$ is the change of concentration in the basolateral chamber over time.

### 2.10. Determination of the passive permeability coefficient ($P_{app}$)

hCMEC/D3 were seeded at $3 \times 10^3$ cells/cm$^2$ in pre-coated 24-transwells with 0.4 μm polyethylenterephthalate (PET) membrane inserts (cellQART, Northeim, Germany; 9320414) and cultured for 7 days. Following, cells were treated with the glycol ethers (2 mM) or the β-metabolites (0.1 mM), as well as with 10 μg/mL LY, 10 μg/mL dextran 40 (ThermoFisher Scientific; D182), 10 μM metoprolol (Sigma; PHR1076), or 10 μM diclofenac (Sigma; 93484) as reference compounds with known BBB-permeation. Incubations were held in a humidified incubator (37 °C, 5 % $CO_2$) on an orbital shaker (100 rpm; Eppendorf; New Brunswick S41i). After 2 h, samples of 30 μL were collected from the apical and basolateral chambers and concentrations either quantified using analytical analysis (for the glycol ethers, β-metabolites, metoprolol, diclofenac) or by measuring the fluorescence applying standard curves (for LY and dextran 40). The apparent permeability ($P_{app}$) was calculated according to Eq. (1) in Section 2.9. Concentrations were corrected by the total recovery considering binding effects. The recovery in percentage was calculated as:

$$Recovery(\%) = \frac{(C_A \quad [\mu g/mL] \quad \times V_A[cm^3]) + (C_B \quad [\mu g/mL] \times V_B[cm^3])}{C_{A0} \quad [\mu g/mL] \times V_A[cm^3]} \times \quad 100 \qquad (2)$$

where $C_A$ and $C_B$ are the final concentrations of compounds in the apical and basolateral chamber, respectively, $C_{A0}$ is the initial concentration in the apical compartment, and $V_A$ and $V_B$ are the apical (0.1 cm$^3$) and basolateral (0.6 cm$^3$) compartment volume, respectively.

### 2.11. In silico permeability prediction

The Unibas toolkit (CDK Toolkit (pharma-te.ch)) (Bendels et al., 2008; Suenderhauf et al., 2012a) and admetSAR 3.0 (admetSAR (ecust.edu.cn)) (Yang et al., 2019) were used to predict blood-brain barrier (BBB) permeance of the compounds. These *in silico* tools use data sets on the passive BBB permeation of drug-like compounds derived from different chemical classes. However, the application of these tools to glycol ethers is unknown. The parameter derived from the Unibas toolkit was the predicted brain/plasma ratio (logBPR), with a given cut-off for likely permeation defined as logBPR > 0.3. The predicted parameter from admetSAR 3.0 was BBB penetration, with the maximum defined as 1.0.

For the correlations, the Pearson correlation coefficient (r) was

**Table 6**
Summarized results for the hepatic enzyme kinetics for the conversion of β-PGEs to β-metabolites.

| | | | | Calculated based on measured Michaelis-Menten-kinetics ($V_{max}/K_m$) | | | Calculated based on measured substrate depletion | | | Calculated based on measured metabolite formation | | | |
|---|---|---|---|---|---|---|---|---|---|---|---|---|---|
| | **$fu_{,inc}$**[b] | **$V_{max}$** [nmol/min/mg] | $K_m$ [μM] | **$CL_{int,\ in\ vitro}$** β-metabolite formation [μL/min/mg] | **Predicted $CL_{int,in\ vivo}$** β-metabolite formation [mL/min/kg] | **Predicted $CL_h$** β-metabolite formation [mL/min/kg] | **$CL_{int,\ in\ vitro}$** substrate depletion [μL/min/mg] | **Predicted $CL_{int,in\ vivo}$** substrate depletion [mL/min/kg] | **Predicted $CL_h$** substrate depletion [mL/min/kg] | **$CL_{int,\ in\ vitro}$** β-metabolite formation [μL/min/$10^6$ cells] | **$CL_{int,\ in\ vitro}$** β-metabolite formation [μL/min/mg] | **Predicted $CL_{int,in\ vivo}$** β-metabolite formation [mL/min/kg] | **Predicted $CL_h$** β-metabolite formation [mL/min/kg] |
| **S9 fraction** | | | | | | | | | | | | | |
| β-PGME → 2-MPA[a] | 0.87 | 1.04 ± 0.28 | 5572 ± 2171 | 0.19 ± 0.03 | 0.60 ± 0.09 | 0.36 ± 0.05 | 3.80 ± 2.14 | 11.8 ± 6.67 | 5.00 ± 2.52 | ND | 40.9 ± 5.19 | 127 ± 16.1 | 16.4 ± 0.47 |
| β-PGEE → 2-EPA | ND | ND | ND | ND | ND | ND | ND | ND | ND | ND | ND | ND | ND |
| β-PGBE → 2-BPA | 0.90 | 1.51 ± 0.15 | 117 ± 45.9 | 14.5 ± 5.63 | 45.1 ± 17.5 | 10.9 ± 1.81 | 7.26 ± 2.01 | 22.6 ± 6.25 | 7.58 ± 1.38 | ND | 58.9 ± 12.5 | 183 ± 38.9 | 17.0 ± 0.66 |
| β-PGPhE → 2-PhPA | 0.88 | 6.16 ± 1.23 | 166 ± 53.6 | 40.2 ± 6.50 | 125 ± 20.2 | 14.8 ± 0.70 | 7.50 ± 0.80 | 23.3 ± 2.49 | 6.64 ± 0.48 | ND | 104 ± 5.33 | 323 ± 16.6 | 18.0 ± 0.12 |
| **3D HepaRG** | | | | | | | | | | | | | |
| β-PGME → 2-MPA[a] | 0.94 | ND | ND | ND | ND | ND | ND | ND | ND | 9.34 ± 0.83 | 9.62 ± 0.85[b] | 28.2 ± 2.50 | 9.07 ± 0.44 |
| β-PGEE → 2-EPA | 0.93 | ND | ND | ND | ND | ND | ND | ND | ND | 16.6 ± 2.89 | 17.1 ± 2.98[c] | 50.1 ± 8.73 | 13.3 ± 0.90 |
| β-PGBE → 2-BPA | 0.91 | ND | ND | ND | ND | ND | ND | ND | ND | 3.55 ± 0.91 | 3.66 ± 0.94[c] | 10.7 ± 2.74 | 4.47 ± 0.89 |
| β-PGPhE → 2-PhPA | 0.88 | ND | ND | ND | ND | ND | ND | ND | ND | 5.92 ± 0.10 | 6.10 ± 0.10[c] | 17.9 ± 0.31 | 5.77 ± 0.07 |

ND: not determined.
The β-PGEs are ordered by increasing lipophilicity (based on logP) from top to bottom. Abbreviations: $fu_{,inc}$: incubational binding; Vmax: maximum reaction rate; Km: Michaelis-Menten-Constant; CLint, in vitro: hepatic intrinsic clearance *in vitro; CLint, in vivo: hepatic intrinsic clearance in vivo; CLh: hepatic organ clearance.*

[a] From Werner et al. (2024).

[b] Data calculated using QIVIVE (qivivetools.wur.nl).

[c] Converted from 9.34 ± 0.83 μL/min/$10^6$ cells, using 117.5 × $10^6$ cells/g liver and 121 mg S9 protein/g liver.

calculated using Graphpad prism (GraphPad Software, San Diego, CA, USA; Version 10.0.2). The following classifications were considered: 0.00–0.30 (negligible), 0.30–0.50 (low), 0.50–0.70 (moderate), 0.70–0.90 (high), 0.90–1.00 (very high) (Mukaka, 2012).

### 2.12. Chemical analytical methods

Glycol ether concentrations were quantified with gas chromatography (GC) with MS detection. The samples were injected into a GC (Agilent; 6890N) equipped with a capillary column (Rxi-624Sil, 60 m, 0.25 mm ID, 1.4 µm, Restek, Bad Soden, Germany) coupled to the MS (5973 Network mass selective detector, Agilent) with a data acquisition software (Agilent MassHunter Quantitative Analysis 10.0).

Alkoxy propionic acid (β-metabolites) concentrations were quantified with a high-performance liquid chromatography (HPLC) with quadrupole mass spectrometer detection (MS/MS). The samples were injected into the HPLC (1200 Series Gradient HPLC system, Agilent, Santa Clara, CA, USA) equipped with a C18 column (InfinityLab Poroshell 120 CS-C18 column (2.1 × 50 mm, 2.7 µm), Agilent; 699775942) connected to the MS/MS in electrospray ionization (ESI) mode (Triple Quadrupole 6475 mass spectrometer, Agilent) with a data acquisition software (MassHunter Quantitative Analysis 10.1, Agilent).

Diclofenac and metoprolol concentrations were quantified with a high-performance liquid chromatography (HPLC) with quadrupole mass spectrometer detection (MS/MS). The samples were injected into the HPLC (1260 Infinity II Series Gradient HPLC system, Agilent, Santa Clara, CA, USA) equipped with a C8 column (InfinityLab Poroshell 120 EC-C8 column (2.1 × 50 mm, 2.7 µm), Agilent; 699775906) connected to the MS/MS in electrospray ionization (ESI) mode (Ultivo Triple Quadrupole 6465BA mass spectrometer, Agilent) with a data acquisition software (MassHunter Quantitative Analysis 10.2, Agilent).

Detailed information on the chemical analytical methods is provided in the Supplementary (Supplementary Tables 4, 5).

### 2.13. Calculation of the in vitro clearance and processing to hepatic organ clearance

The *in vitro* $CL_{int}$ for the substrate depletion and the β-metabolite formation was determined according to Eq. (3) for the S9 incubations and Eq. (4) for the cellular incubations (Obach et al., 1997):

$$CL_{int,in\ vitro}\ [\mu L/min/mg] = \frac{\pm k\ [1/min] \times volume[\mu L]}{S9protein[mg]} \quad (3)$$

$$CL_{int,in\ vitro}\ [\mu L/min/Million\ cells] = \frac{\pm k\ [1/min] \times volume[\mu L]}{cell\ number[Million\ cells]} \quad (4)$$

where the elimination (-k) and the formation constant (k) were derived from the slope of the linear regression from the ln-transformed % of solvent remaining *versus* the incubation time and the ln-transformed β-metabolite concentration *versus* the incubation time, respectively.

The *in vitro* $CL_{int}$ for the S9 incubations was calculated as following:

$$CL_{int,in\ vitro}\ [\mu L/min/mg] = \frac{V_{max}\ [nmol/min/mg]}{K_m\ [\mu M]} \quad (5)$$

where $V_{max}$ is the maximum velocity and $K_m$ the Michaelis-Menten-Constant, both predicted from GraphPad Prism.

The *in vivo* hepatic intrinsic clearance ($CL_{int,\ in\ vivo}$) was calculated using physiological scaling factors for hepatocellularity (Barter et al., 2006; Musther et al., 2017), for the protein (Houston and Galetin, 2008), and liver weight (Davies and Morris, 1993) according to Eqs. (6) and (7):

$$CL_{int,in\ vivo}\ [mL/min/kg] = CL_{int,in\ vitro} \times 121\ \frac{mgS9protein}{gliver} \times 25.7\ \frac{gliver}{kg\ bodyweight} \quad (6)$$

$$CL_{int,in\ vivo}\ [mL/min/kg] = CL_{int,in\ vitro} \times 117.5\ \frac{10^6 cells}{gliver} \times 25.7\ \frac{gliver}{kg\ bodyweight} \quad (7)$$

The *in vitro* hepatic organ clearance ($CL_h$) was predicted using the well-stirred liver model according to Eq. (8) (Pang and Rowland, 1977):

$$CL_h\ [mL/min/kg] = \frac{Q_H\ [mL/min/kg] \times CL_{int,in\ vivo}\ [\mu L/min/kg] \times \frac{f_{u,\ b}}{f_{u,inc}}}{Q_H\ [mL/min/kg] + CL_{int,in\ vivo}\ [\mu L/min/kg] \times \frac{f_{u,\ b}}{f_{u,inc}}} \quad (8)$$

where $Q_H$ is the hepatic blood flow (20.7 mL/min/kg) (Riley et al., 2005). Incubational binding for the test system ($fu_{,inc}$) and plasma binding ($fu_{,b}$) was predicted using a QIVIVE platform (qivivetools.wur.nl) (Berezhkovskiy, 2004; Jones and Rowland-Yeo, 2013; Lobell and Sivarajah, 2003), taking into account the physicochemical properties of the compounds. For the S9 incubations, the S9 protein concentration was considered and the Hallifax and Houston method applied (Hallifax and Houston, 2006). For the 3D HepaRG experiments, the cell concentration was considered and the Kilford method applied (Kilford et al., 2008).

### 2.14. Statistical analysis

Data representation and statistical analysis were performed using Microsoft Excel (Microsoft, Redmond, WA) and GraphPad Prism. Data are expressed as mean values ± SD. For the statistical analysis of two groups, the student's *t*-test was used. One-way ANOVA was used for statistical analysis of multiple conditions. $p < 0.05$ was considered as significant (*, $p \leq 0.05$; **, $p \leq 0.01$; ***, $p \leq 0.001$, ****, $p \leq 0.0001$).

## 3. Results

### 3.1. The toxicity of propylene glycol ethers depends on their carbon chain length

To assess the cytotoxicity of the glycol ethers and the alkoxy propionic acids (β-metabolites) on 3D HepaRG and hCMEC/D3, we exposed them over either 48 h or 7 days. Relative cell viability, measured as cellular ATP content, indicated a trend towards an increasing toxicity of the glycol ethers, in accordance with their carbonic chain length and lipophilicity (logP) (Table 5). The 3D HepaRG and hCMEC/D3 cultures were fairly resistant to the treatments with $EC_{50}$ values in the millimolar range. Generally, $EC_{50}$ values for all compounds were lower after 7 days than after 48 h of treatment. We observed higher toxicity for the β-isomer PGEs (β-PGE) than for the isomer mixtures, which are primarily composed of the α-isomer (> 95.5 %) and a small fraction of the β-isomer (< 0.5 %). This was true in 3D HepaRG and particularly pronounced in hCMEC/D3.

Regarding the toxicity of the β-metabolites, we did not observe any discernible trend with respect to their carbonic chain length and lipophilicity. 2-EPA and 2-PhPA showed a low toxic potential on the 3D HepaRG, precluding the calculation of $EC_{50}$ values. In contrast, hCMEC/D3 cells were highly sensitive to the β-metabolites, with similar $EC_{50}$ values for all of them. Moreover, all β-metabolites (except 2-PhPA that was approximately twofold less toxic than β-PGPhE) were more toxic than their parent β-PGEs.

All cytotoxicity curves can be found in the Supplementary (Supplementary Figs. 5–8).

**Table 5**
Summarized cytotoxicity results for the glycol ethers, ethanol, and β-metabolites.

| | Carbonic chain length | logP[b] | 3D HepaRG (48 h) | | 3D HepaRG (7 d) | | hCMEC/D3 (48 h) | |
|---|---|---|---|---|---|---|---|---|
| | | | $EC_{50}$ [mM] | 95 % CI | $EC_{50}$ [mM] | 95 % CI | $EC_{50}$ [mM] | 95 % CI |
| EGME | C = 3 | − 0.80 | 326[a] | 261–397[a] | 171[a] | 139–205[a] | 278 | 128–426 |
| PGME | C = 4 | − 0.49 | 226[a] | 194–262[a] | 96[a] | 73–126[a] | 259 | 238–280 |
| β-PGME | C = 4 | − 0.49 | 162[a] | 146 –183[a] | 86[a] | 75–99[a] | 143 | 127–160 |
| PGEE | C = 5 | 0.30 | 90 | 65–118 | 40 | 24–59 | 188 | 166–214 |
| β-PGEE | C = 5 | 0.20* | 54 | 41 – 68 | 35 | 21–50 | 21 | 18– 25 |
| PGPE | C = 6 | 0.70 | 50 | 44 – 55 | 16 | 10–23 | 60 | 54–68 |
| PGBE | C = 7 | 1.15 | 31 | ND | 10 | 5–13 | 44 | 38–50 |
| β-PGBE | C = 7 | 1.10* | 27 | 22–34 | NA | NA | NA | NA |
| PGPhE | C = 9 | 1.50 | 9 | ND | 1 | ND | 7 | ND |
| β-PGPhE | C = 9 | 1.60* | 5 | ND | 1 | ND | 9 | ND |
| Ethanol | C = 2 | | 610[a] | 464–898[a] | NA | NA | > 1000 | ND |
| 2-MAA | C = 3 | − 0.30 | 11[a] | 5–15[a] | 9[a] | 8–10[a] | 14 | 12–15 |
| 2-MPA | C = 4 | 0.10* | 46[a] | ND | 26[a] | 23–30[a] | 30 | 28–37 |
| 2-EPA | C = 5 | 0.40* | ND | ND | ND | ND | 25 | 22–30 |
| 2-PPA | C = 6 | 1.00 | 504 | ND | 20 | 6–29 | 18 | 14–23 |
| 2-BPA | C = 7 | 1.30* | 40 | 29–195 | 17 | 13–20 | 15 | 14–17 |
| 2-PhPA | C = 9 | 1.70* | ND | ND | ND | ND | 18 | 17–20 |

Cellular ATP decrease assessed on 3D HepaRG cultures and hCMEC/D3 upon 48 h and 7 days of exposure expressed as $EC_{50}$ values and the corresponding 95 % confidence interval (CI). ND: not determinable. NA: not available.
Time in () indicates the duration of the incubation with the compound. Abbreviations: logP: octanol-water partition coefficient. The glycol ethers and β-metabolites are ordered by increasing lipophilicity (based on logP) from top to bottom.
[a] From Werner et al. (2024).
[b] Data retrieved January 12, 2024, from Pubchem. PubChem (nih.gov).
* Computed data.

### 3.2. The in vitro clearance of β-isomer propylene glycol ethers depends on their carbon chain length

We determined the Michaelis-Menten kinetic parameters (Michaelis-Menten-Constant ($K_m$) and maximum reaction rate ($V_{max}$)) using the S9 incubations (Fig. 2A, values summarized in Table 6) to evaluate enzymatic kinetic parameters of the β-PGEs and thus enzyme saturation concentrations. The $V_{max}$ value was remarkably higher for β-PGPhE than for β-PGBE, resulting in a higher calculated *in vitro* hepatic intrinsic clearance ($CL_{int}$) ($V_{max}/K_m$) for β-PGPhE than for β-PGBE. Combining the outcome with our previously reported results for β-PGME (Werner et al., 2024), we could rank the β-PGEs based on their carbonic chain length. Specifically, we noticed a pattern for increasing calculated *in vitro* $CL_{int}$ values ($V_{max}/K_m$), simultaneously reflected in lower $K_m$ values and higher $V_{max}$ values, dependent on the chain length of the β-PGEs (β-PGPhE > β-PGBE > β-PGME).

Next, we calculated the *in vitro* $CL_{int}$ based on the measured depletion of the β-PGEs (substrate depletion) and based on the corresponding β-metabolite formation (Fig. 2B, Table 6, Supplementary Fig. 9A). Notably, the clearance determined by measuring the formed β-metabolites 2-BPA and 2-PhPA was 8 and 14 times higher than the clearance determined based on substrate depletion for β-PGBE and β-PGPhE, respectively. Again, ranking of the measured *in vitro* $CL_{int}$ values according to the β-PGE chain length was possible for the obtained values.

We also determined the *in vitro* $CL_{int}$ for the β-metabolite formation of 2-EPA, 2-BPA, and 2-PhPA from β-PGEE, β-PGBE, and β-PGPhE (Fig. 2C, Table 6, Supplementary Fig. 9B) using a 3D HepaRG model. We encountered analytical issues, as only a small quantity of the β-PGEs was metabolized and the obtained depletion curves could not be reliably measured with the analytical methods. Therefore, the clearance based on substrate depletion was not determined. Artifacts due to stability, adsorption, or evaporation of the β-PGEs and the β-metabolites over time are not expected based on additional tests (Supplementary Fig. 10, 11). Based on our findings and considering our previously reported results for β-PGME, no ranking for the *in vitro* $CL_{int}$ based on the chain length of the β-PGEs could be determined in the 3D HepaRG incubations. In addition, the determined *in vitro* $CL_{int}$ values for β-metabolite formation using the 3D HepaRG were notably lower (approximately 2 to 17-fold) than the *in vitro* $CL_{int}$ values for β-metabolite formation obtained from S9.

The calculated hepatic organ clearance ($CL_h$) based on the calculated *in vitro* $CL_{int}$ ($V_{max}/K_m$) values and the measured *in vitro* $CL_{int}$ values is summarized in Table 6. The predicted $CL_h$ values were within threefold agreement for the S9 and 3D HepaRG, except for the $CL_h$ calculated on the *in vitro* $CL_{int}$ ($V_{max}/K_m$) for 2-MPA. Reiterating the obtained $CL_h$ values, the same ranking pattern was observed as for the *in vitro* $CL_{int}$ based on the calculated *in vitro* $CL_{int}$ ($K_m/V_{max}$) and measured *in vitro* $CL_{int}$ in S9 (β-metabolite formation). On the contrary, no trends within the β-PGEs for calculations based on the measured *in vitro* $CL_{int}$ in S9 (substrate depletion) and the measured *in vitro* $CL_{int}$ 3D HepaRG (β-metabolite formation) were observed.

### 3.3. Propylene glycol ethers and their β-metabolites permeate through the blood-brain barrier

The hCMEC/D3 cell line expressed endothelial markers comparable to an *in vitro* primary cell model (HBMVEC) as determined by immunostaining with antibodies towards CD31 and ZO-1 (Fig. 3A, Supplementary Fig. 12). Considering their function, the hCMEC/D3 built a tight endothelial barrier with a measured *in vitro* passive permeability ($P_{app}$, A–B) for Lucifer yellow (LY; 0.5 kDa) of $0.92 \pm 0.10 \times 10^{-3}$ cm/min. None of the tested glycol ethers or β-metabolites impaired the barrier function as determined by the *in vitro* $P_{app}$ of LY after incubation of hCMEC/D3 (Fig. 3B).

Despite the tightness of the cellular barrier, permeation of the glycol ethers through the hCMEC/D3 was rapid with *in vitro* $P_{app}$ values of 1.6 – $2.9 \times 10^{-3}$ cm/min as shown in Fig. 3C. Acceptable assay recoveries were obtained for all compounds with total recoveries between 59.0 % and 101 % (Supplementary Fig. 13). No trend based on lipophilicity was observed. The *in vitro* $P_{app}$ values of the β-metabolites were generally slightly lower than the values observed for the glycol ethers, except for 2-MAA, which exhibited a $P_{app}$ value of $3.00 \pm 0.5 \times 10^{-3}$ cm/min. All values are summarized in Table 7.

Comparing the measured *in vitro* $P_{app}$ values with the *in silico* permeability predictions (logBPR, BBB penetration), we observed poor correlations for the glycol ethers and β-metabolites (Supplementary Fig. 14). However, strong correlations (Pearson correlation coefficient $r \geq 0.89$) between the permeability predictions and the experimental

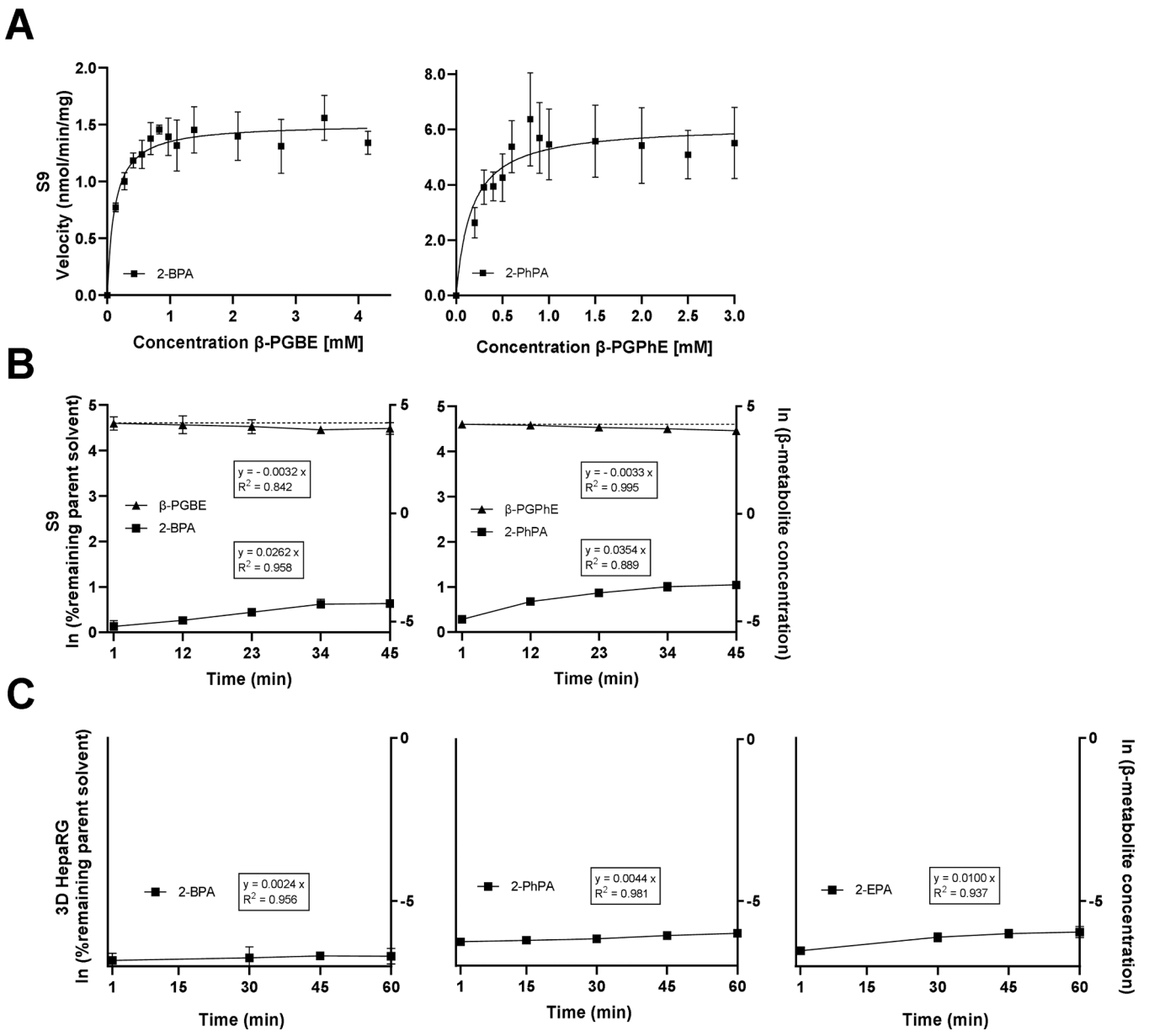


**Fig. 2.** **(A)** Representative velocity against substrate concentration plot for Michaelis-Menten kinetics in S9 incubations. 2-BPA and 2-PhPA were quantified using HPLC-MS/MS. The Michaelis-Menten curve was fitted to the data using Graphpad Prism and $K_m$ and $V_{max}$ predicted. Data points represent means ± SD of N = 3 independent incubations with 2 technical replicates. **(B)** Ln of % remaining parent solvent (▲) and ln of β-metabolite concentration (■) *versus* time profile in S9 incubations. **(C)** Ln of β-metabolite concentration (■) *versus* time profile in 3D HepaRG. The *in vitro* $CL_{int}$ was calculated from the slope. Data points represent means ± SD of N = 2–3 independent incubations summarizing calculated slopes derived from each single graph. The dotted line represents the parent value at time-point 1 min.

values were obtained for the reference compounds dextran 40, diclofenac, LY, and metoprolol.

In general, BBB penetration predictions from admetSAR showed values ranging from 0.55 to 0.93 for the glycol ethers, while the values for the β-metabolites were comparable with 0.73–0.88 (Table 7). In contrast to a predicted likely permeation of the glycol ethers applying the Unibas toolkit, the values for the β-metabolites were below the defined threshold (< 0.3) for likely permeation. This contradicts the observed high *in vitro* permeability of the β-metabolites. Moreover, comparisons with the physicochemical parameters of the compounds showed a positive correlation between the permeability of the reference compounds and their lipophilicity (AlogP, logP). In contrast, the molecular weight (MW), fractional charge weighted partial positive surface area / total molecular surface area (FPSA-3), and number of hydrogen bond acceptors (nHBAcc) showed negative correlations.

Similarly, we noticed a moderate positive correlation for the glycol ethers with AlogP (admetSAR) and logP (Pubchem), and a moderate negative correlation with FPSA-3. The predicted AlogP from the Unibas toolkit exhibited a poor correlation. Contrary to the reference compounds, we observed a moderate positive relationship between the *in vitro* $P_{app}$ and MW. For the β-metabolites, we found a moderate negative relationship between the permeability and lipophilicity (logP, AlogP), and a moderate positive correlation for FPSA-3, which differed from the findings for the reference compounds and the glycol ethers. Only the moderate negative correlation with MW was consistent with the findings for the reference compounds. Correlations for nHBAcc could not be performed for the glycol ethers and the β-metabolites because of identical values within the set.

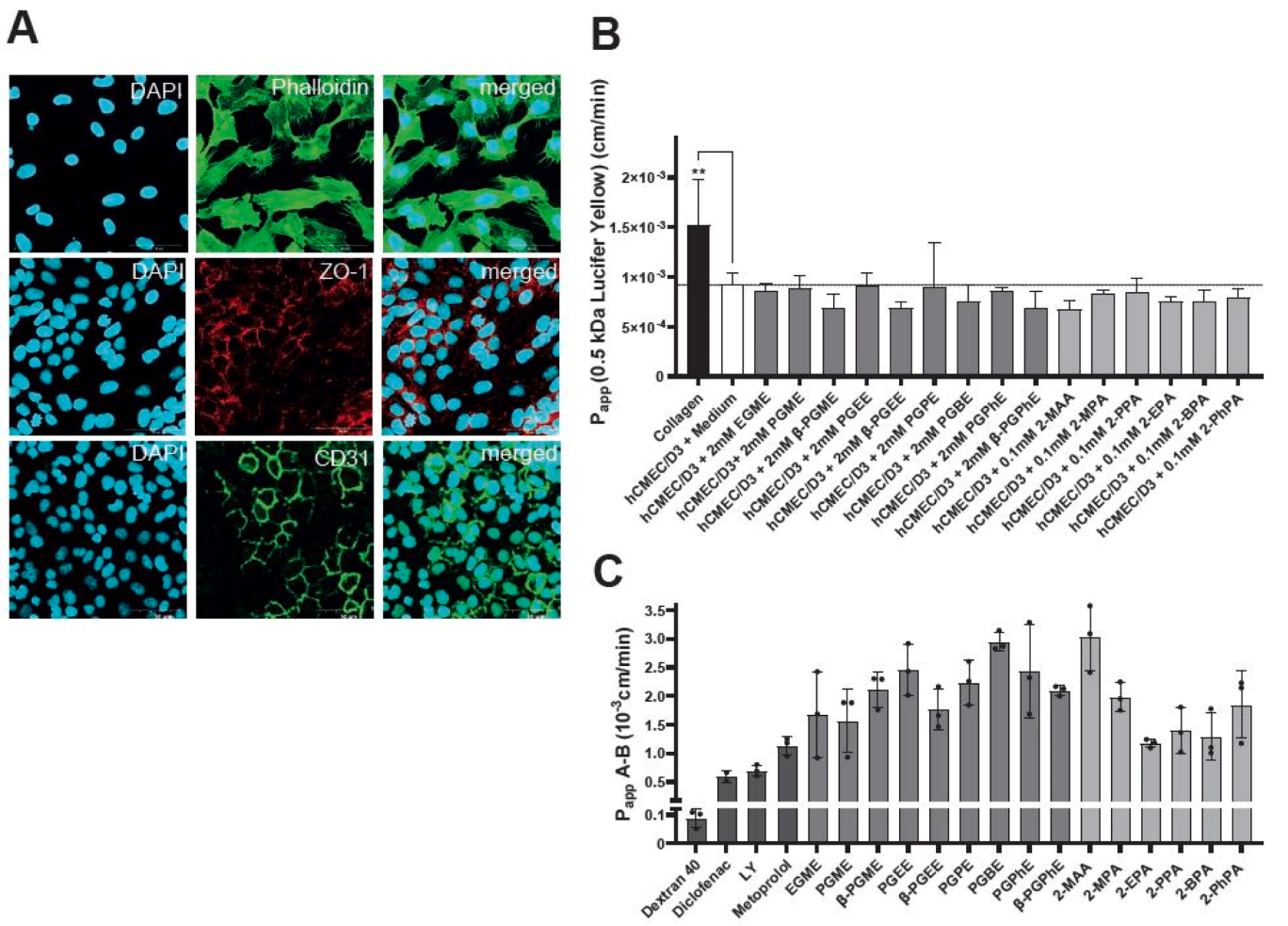


**Fig. 3.** **(A)** Expression of BBB and endothelial cells markers in the hCMEC/D3 cell line. Immunostainings of Phalloidin (green), ZO-1 (red), CD31 (green), and DAPI nuclear counter-staining (blue). Scale bar: 50 μm. **(B)** Assessment of the barrier tightness after exposure to the glycol ether and the β-metabolites for 48 h. The flux, reported as passive permeability ($P_{app}$) coefficient, was determined in apical-to-basolateral direction for the fluorescent labeled marker Lucifer yellow (LY) 0.5 kDa. N = 3 independent biological repeats with 2 technical replicates. Graphs represent means ± SD; statistical analysis based on one-way ANOVA followed by Dunnett's pairwise comparison: **, $p \leq 0.01$. **(C)** Permeation ($P_{app}$) of the glycol ethers, β-metabolites, and the reference compounds through the hCMEC/D3. N = 3 independent biological repeats with 2 technical replicates, N = 2 independent biological repeats with 2 technical replicates for Diclofenac. Graphs represent means ± SD. For (B) and (C), the values are ordered by increasing lipophilicity (based on logP) from left to right.

### *3.4. BBB and brain in vitro models express ADH and ALDH*

We performed experiments to elucidate the presence of the relevant enzymes ADH1 and ALDH2 on the gene and protein level in the CNS models (*in vitro* BBB: hCMEC/D3, HBMVEC; BrainSpheres) and human brain total RNA as comparator. Based on q-RT-PCR results (Fig. 4A), ALDH2 showed the highest gene expression level across all models. The expression of ADH1B and ADH1C was similar in all models, whereby the highest expression for ADH1C was found for the BrainSpheres. Interestingly, ADH1A expression was only measurable for the BrainSpheres.

Furthermore, we confirmed the presence of the enzymes on the protein level using immunostaining (ADH1A/B/C and ALDH2) and Western blot (ALDH2) in lysates derived from hCMEC/D3, HBMVEC, and BrainSpheres (Fig. 4 B/C, Supplementary Fig. 15). The signal mean intensity relative to GAPDH was the highest for the BrainSpheres (ALDH2: 1.98 ± 0.58), followed by HBMVEC (ALDH2: 1.14 ± 0.38) and hCMEC/D3 (ALDH2: 0.97 ± 0.30) (Fig. 4D).

### *3.5. β-isomer propylene glycol ethers are metabolized by the liver and in the CNS*

After exposure to β-PGEs, β-metabolite formation over 24 h was successfully demonstrated for the 3D HepaRG, 3D primary human hepatocytes (pHH), hCMEC/D3, and HBMVEC as illustrated in Fig. 5A. As similar β-PGE concentrations were used, we calculated ratios comparing β-metabolite formation within the specific cell models, with the 3D HepaRG serving as the benchmark standard (Table 8). Remarkably, we observed a linear β-metabolite formation occurring within the first hour for all four systems, which then reached a steady state within 24 h.

For hepatic metabolism, we detected similar or lower metabolic rates in 3D HepaRG than in 3D pHH but both *in vitro* liver systems metabolized the β-PGEs within twofold agreement.

Regarding the extra-hepatic metabolism in the BBB *in vitro* models, similar amounts of 2-MPA and 2-EPA were produced by both hCMEC/D3 and HBMVEC. We could not detect 2-BPA and 2-PhPA formation, likely due to the analytical limit of detection. The β-metabolite formation in hCMEC/D3 and HBMVEC was approximately 16–33 % and 10–20 % of hepatic metabolism, respectively.

Also, exposure of the BrainSpheres to β-PGME and β-PGEE over 6 h showed the successful formation of the β-metabolites 2-MPA and 2-EPA (Fig. 5B). We measured an approximately threefold higher formation for 2-EPA (12.87 ± 3.90 pmol/μg) than 2-MPA (4.30 ± 1.33 pmol/μg).

**Table 7**
Overview of physicochemical parameters, predicted blood-brain barrier permeability (logBPR, BBB penetration), and measured *in vitro* $P_{app}$.

| | MW[a] (g/mol) | logP[a] | AlogP[b] | tPSA[b] | FPSA-3[b] | nHBAcc[b] | logBPR[b] | AlogP[c] | BBB penetration[c] | $P_{app}$ *in vitro* ($10^{-3}$ cm/min) |
|---|---|---|---|---|---|---|---|---|---|---|
| **EGME** | 76.09 | − 0.80 | − 0.4889 | 29.46 | 0.0479 | 2 | 0.50 | − 0.37 | 0.93 | 1.7 ± 0.6 |
| **PGME** | 90.12 | − 0.49 | − 0.4996 | 29.46 | 0.046 | 2 | 0.50 | 0.01 | 0.88 | 1.6 ± 0.4 |
| **β-PGME** | 90.12 | − 0.49 | − 0.4996 | 29.46 | 0.0426 | 2 | 0.50 | 0.01 | 0.85 | 2.1 ± 0.3 |
| **PGEE** | 104.2 | 0.30 | − 0.2492 | 29.46 | 0.0362 | 2 | 0.47 | 0.40 | 0.90 | 2.5 ± 0.4 |
| **β-PGEE** | 104.2 | 0.20 | − 0.2492 | 29.46 | 0.0363 | 2 | 0.47 | 0.40 | 0.85 | 1.8 ± 0.3 |
| **PGPE** | 118.2 | 0.70 | − 0.8270 | 29.46 | 0.0353 | 2 | 0.54 | 0.79 | 0.88 | 2.2 ± 0.3 |
| **PGBE** | 132.2 | 1.15 | − 1.115 | 29.46 | 0.0333 | 2 | 0.57 | 1.18 | 0.90 | 2.9 ± 0.1 |
| **β-PGBE** | 132.2 | 1.10 | − 1.115 | 29.46 | 0.0331 | 2 | 0.57 | 1.18 | 0.85 | NA |
| **PGPhE** | 152.2 | 1.50 | 0.3547 | 29.46 | 0.0446 | 2 | 0.40 | 1.59 | 0.55 | 2.4 ± 0.7 |
| **β-PGPhE** | 152.2 | 1.60 | 0.3547 | 29.46 | 0.0429 | 2 | 0.40 | 1.45 | 0.58 | 2.1 ± 0.1 |
| **2-MAA** | 90.08 | − 0.30 | − 0.4934 | 46.53 | 0.0466 | 3 | 0.23 | − 0.28 | 0.80 | 3.0 ± 0.5 |
| **2-MPA** | 104.1 | 0.10 | − 0.3974 | 46.53 | 0.0399 | 3 | 0.22 | 0.11 | 0.80 | 2.0 ± 0.2 |
| **2-EPA** | 118.1 | 0.40 | − 0.1470 | 46.53 | 0.0344 | 3 | 0.19 | 0.50 | 0.88 | 1.2 ± 0.1 |
| **2-PPA** | 132.2 | 1.00 | − 0.7248 | 46.53 | 0.0266 | 3 | 0.26 | 0.89 | 0.83 | 1.4 ± 0.3 |
| **2-BPA** | 146.2 | 1.30 | − 1.0128 | 46.53 | 0.0237 | 3 | 0.29 | 1.28 | 0.83 | 1.3 ± 0.3 |
| **2-PhPA** | 166.2 | 1.70 | 0.4569 | 46.53 | 0.0533 | 3 | 0.11 | 1.54 | 0.73 | 1.9 ± 0.4 |
| **Dextran 40** | 504.4 | − 7.20 | − 6.284 | 276.52 | 0.0622 | 16 | − 2.72 | − 7.73 | 0.53 | 0.1 ± 0.0 |
| **Diclofenac** | 296.1 | 4.40 | 1.830 | 49.33 | 0.034 | 3 | − 0.10 | 4.36 | 0.58 | 0.6 ± 0.1 |
| **Lucifer yellow** | 442.3 | ND | ND | 249.68 | 0.0479 | 13 | ND | − 7.58 | 0.60 | 0.7 ± 0.1 |
| **Metoprolol** | 267.4 | 1.90 | − 0.0334 | 50.72 | 0.0399 | 4 | 0.10 | 1.61 | 0.75 | 1.1 ± 0.1 |

NA: not available, ND: not determinable.
Abbreviations: MW: molecular weight; logP: octanol-water partition coefficient; AlogP: Ghose-Crippen LogKow; tPSA: topological polar surface area; FPSA-3: fractional charge weighted partial positive surface area / total molecular surface area; nHBAcc: number of hydrogen bond acceptors; logBPR: predicted brain/plasma ratio; $P_{app}$: *in vitro passive permeability coefficient.*
[a] Data retrieved January 12 and June 18, 2024, from Pubchem. PubChem (nih.gov).
[b] Data retrieved June 18, 2024, from Unibas toolkit.
[c] Data retrieved June 18, 2024, from admetSAR 3.0.

## 4. Discussion

In this work, we applied *in vitro* methods to assess the neurotoxic potential of propylene glycol ethers (PGEs), consisting of mixtures of secondary (α-isomer) and primary (β-isomer, generally < 5 %) alcohols, after systemic exposure. We focused on the hepatic metabolism of the β-isomers of PGEs (β-PGEs) forming alkoxy propionic acids (β-metabolites), which might lead to neurotoxic effects in humans, and studied the ability of PGEs to damage or cross the blood-brain barrier (BBB). In addition, we hypothesized that the formation of the potential neurotoxic β-metabolites from PGEs might occur not only in the liver but also in the central nervous system (CNS).

We embarked on determining the presence and activity of the key metabolic enzymes alcohol dehydrogenase (ADH1) and aldehyde dehydrogenase (ALDH2) in BBB and brain, as *in situ* formation of toxic β-metabolites may contribute to the neurotoxicity of PGEs. Consistent with previous studies using rat, mice, and human brain tissue (Galter et al., 2003; Tsang et al., 2021), we observed low expression of ADH1 in the *in vitro* CNS (BBB and brain) models. However, both ADH1 and ALDH2 enzymes were expressed in all analyzed samples, with the highest expression levels (transcripts and protein) of ALDH2 and ADH1C (gamma subunit) detected in the BrainSpheres. The ranking of relative abundance based on the measured expression levels was generally similar to the one reported in the Human Protein Atlas (proteinatlas.org) (Evelina et al., 2020). In total mRNA, derived from human brain and used as a comparator, ADH1 transcript levels were ranked as follows according to their relative expression: ADH1B > ADH1C > ADH1A. In the *in vitro* CNS models, the expression ranking of the enzyme subunits was slightly different with ADH1C > ADH1B > ADH1A. Although we could not calculate the proportion of metabolism in the BrainSpheres compared to the 3D HepaRG model due to different conditions used, the qualitative assessment clearly demonstrated that the BrainSpheres consisting of neurons, astrocytes, and oligodendrocytes (Pamies et al., 2017) were able to generate β-PGE metabolites. In the past, some *in vitro* studies have shown the presence of ADH in the CNS in a small number of neurons and ADH activity has been described in astrocytes, blood capillaries, and neurons (Zimatkin and Deitrich, 1997). However, the specific cell types responsible for ADH1/ALDH2-mediated glycol ether metabolism in the BrainSpheres need to be further explored.

Based on our results, the brain is not the only CNS-tissue able to metabolize PGEs. Both hCMEC/D3 and primary HBMVEC performed ADH1/ALDH2-mediated metabolism to a similar extent, suggesting active participation of the BBB. The metabolic capacity of the BBB *in vitro* was, as expected, lower than that estimated for the liver with 3D HepaRG; however, our results clearly show the potential of extra-hepatic metabolism for the PGEs in the BBB and in the brain. A possible loss of substrates during the incubation time was not expected based on the demonstrated compound stability over 24 hours performed in this paper (for β-PGEE) and by Werner et al. (2024) (for β-PGME), considering similar experimental conditions for the liver and the BBB models (both 96-well plates). Lastly, it should be noted that extra-hepatic metabolism of the PGEs by other organs possibly enhancing PGE-mediated toxicity cannot be excluded, as ADH1 and ALDH2 expressions were also shown for other human tissues, including the stomach and the lung (Crabb et al., 2004; Jiang et al., 2020). However, in this research, we have only focused on CNS-related metabolism and its relevance for PGE neurotoxicity.

Brain exposure is a pre-requisite for neurotoxicity. Hence, we also investigated the ability of the glycol ethers to cross the BBB. Our data shows that PGEs and their β-metabolites exhibited high permeation through the hCMEC/D3 cell layer, a surrogate of the BBB (Poller et al., 2008; Weksler et al., 2013). The barrier integrity of this *in vitro* BBB model was assessed by determining the apparent permeability coefficients ($P_{app}$) for Lucifer yellow (LY), showing that the BBB model performed similarly to previously reported studies (Choublier et al., 2021; Eigenmann et al., 2013; Poller et al., 2008; Weksler et al., 2013). Furthermore, the $P_{app}$ value for metoprolol was in line with literature (Kim et al., 2024). For Dextran 40, the obtained $P_{app}$ value was notably higher than previously reported by Kim et al. (2024), suggesting lower BBB integrity. However, studies using Dextran 70 kDa (Biemans et al., 2017; Weksler et al., 2013), which was expected to have lower permeability, showed similar $P_{app}$ values to ours, making direct comparisons challenging. With this model we could establish the ability of the PGEs and the β-metabolites as well as ethylene glycol methyl ether (EGME), to

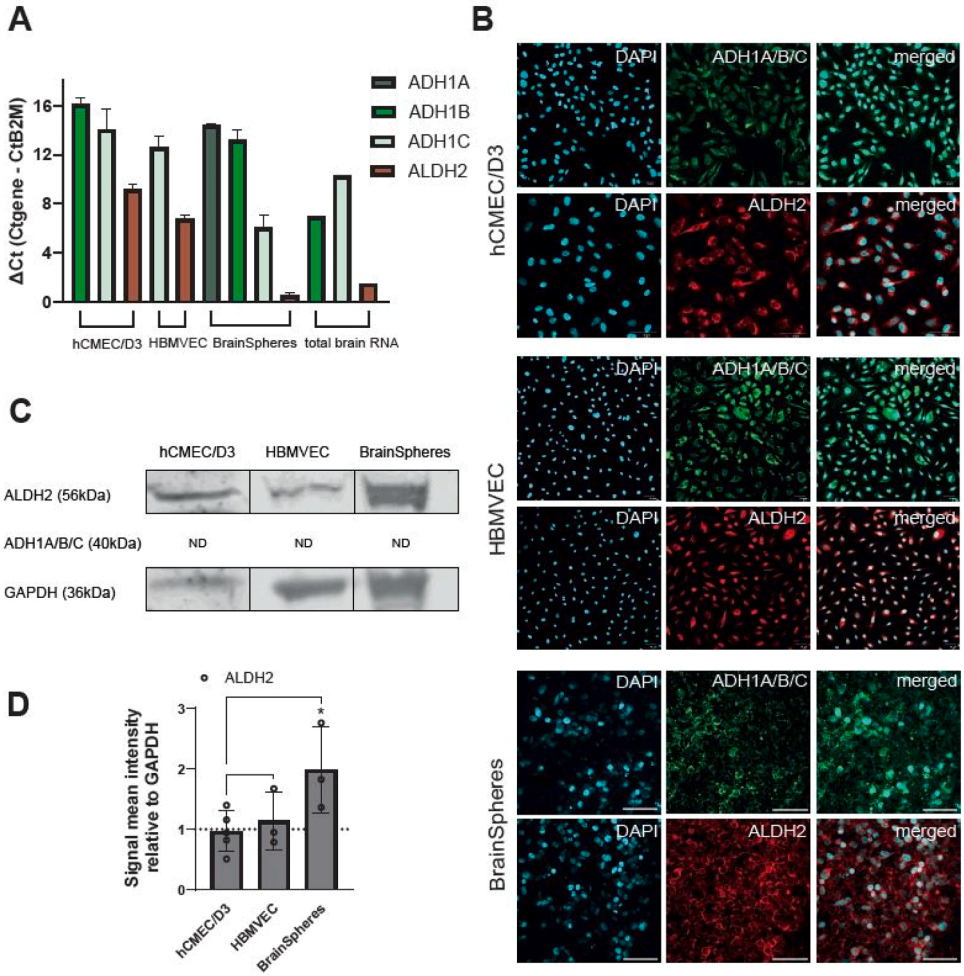


**Fig. 4.** **(A)** Gene expression of ADH1A, ADH1B, ADH1C and ALDH2 in hCMEC/D3, HBMVEC, BrainSpheres, and human brain total RNA was detected using q-RT-PCR; N = 3 independent biological repeats with 2 technical replicates (hCMEC/D3, HBMVEC, BrainSpheres) and N = 1 biological experiment with 2 technical samples (human brain total RNA). Bar graphs represent means ± SD. **(B)** hCMEC/D3, HBMVEC, and BrainSpheres were stained for ADH1A/B/C (green), ALDH2 (red), and counterstained with DAPI/Hoechst (blue). Scale bar: 50 μm. **(C)** Western blot of ALDH2 and GAPDH (loading control) in hCMEC/D3, HBMVEC, and Brainspheres cell lysates. ND: not determinable. **(D)** Signal mean intensity relative to GAPDH for ALDH2 was determined using ImageJ (N = 3–4 independent biological repeats). Bar graphs represent means ± SD; statistical analysis based on Student's unpaired *t*-test: *, $p \leq 0.05$.

cross the BBB and access the brain. All tested chemicals showed permeability values even higher than that of metoprolol, which is clinically known to cause CNS side effects due to its ability to cross the BBB (Shah et al., 2020). To conclude, although our results obtained with the hCMEC/D3 showed to be in the range of other studies, the reduced barrier integrity compared to *in vivo* conditions still needs to be considered as a limitation of the cell line (Biemans et al., 2017).

Although the BBB-permeability of the comparator substances (dextran 40, diclofenac, LY, metoprolol) was in agreement with results obtained *in silico* (logBPR), this was not the case for the glycol ethers and their β-metabolites. For those chemicals, the computer-based model (logBPR) underestimated BBB permeability, probably due to its limited domain of applicability, as the *in silico* tools were developed and validated for drug-like compounds and not for solvents (Bendels et al., 2008; Suenderhauf et al., 2012b). The applicability of the used *in vitro* tools to compounds that are substrates of transporters, e.g. P-glycoprotein, as another important aspect of BBB penetration, remains unclear. However, *in vitro* and *in silico* results consistently showed that BBB-permeability was higher for the parent solvents than for their β-metabolites and independent of the carbon chain lengths. It has been suggested that permeation is not solely dependent on lipophilicity (logP), but also on other key parameters such as molecular weight (MW), polar surface area (tPSA), the number of hydrogen bond acceptors and donors, and ionization (pKa) (Geldenhuys et al., 2015). Although we cannot ascertain which characteristics led to high permeability, our findings for the reference compounds are in concordance with reported data showing a positive correlation with logP and a negative correlation with tPSA, number of hydrogen bond acceptors (nHBAcc), and MW (Waring, 2009). Hence, we conclude that the lower permeability of the β-metabolites compared to their corresponding parent solvents is partly due to differences in lipophilicity. Further studies would be necessary to evaluate the influence of other parameters such as PSA, hydrogen bond donor/acceptor count, tPSA, pka, or MW.

Hepatic metabolism plays a major role in the biotransformation of chemicals, including PGEs. Incubations of 3D HepaRG and subcellular liver S9 fraction with a variety of β-PGEs corroborated our recent work using a similar solvent (Werner et al., 2024). Hence, applying the 3D HepaRG model, we were able to show active metabolism in the cells *via* ADH/ALDH pathway and to generate hepatic clearance data for the β-PGEs. Furthermore, we observed comparable long-term metabolic capacity of 3D HepaRG to that of 3D primary human hepatocytes. As ease-of-use systems like S9 cell fractions are limited by the short functionality of their enzymes (Ingelman-Sundberg and Lauschke, 2021), more complex systems like 3D liver cultures benefit from maintained enzyme functionality over multiple weeks and better represent *in vivo*-like conditions (Bonn et al., 2016; Lübberstedt et al., 2011; Smith

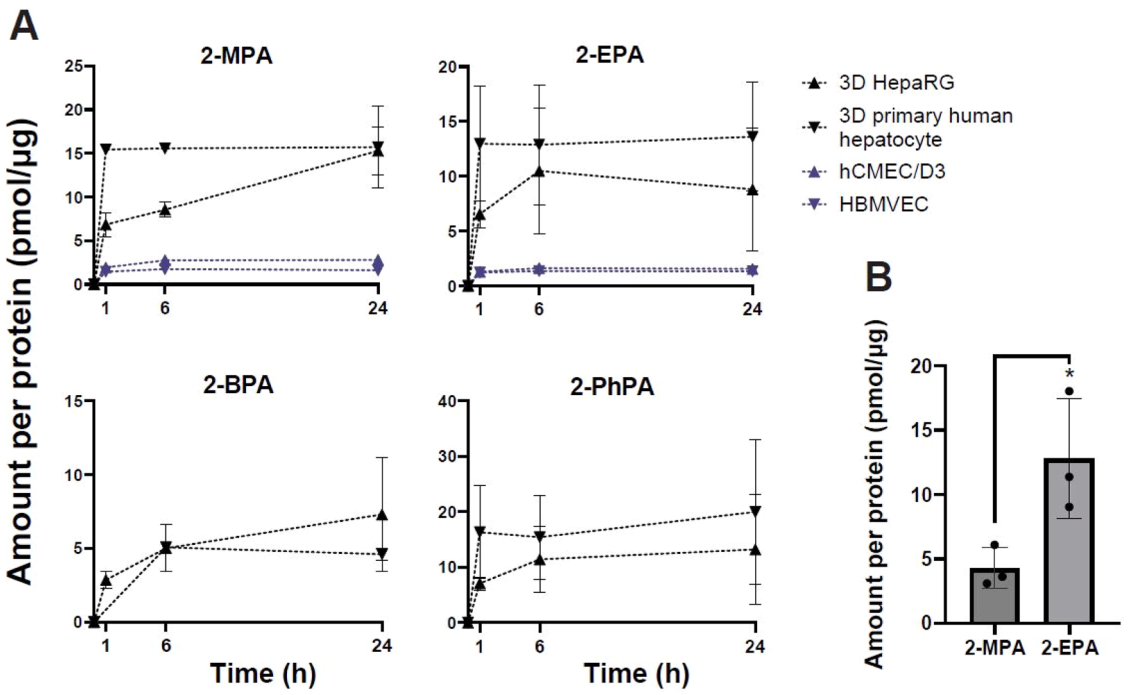


**Fig. 5. (A)** β-metabolite formation-time profiles in 3D HepaRG (▲), 3D primary human hepatocytes (pHH) (▼), hCMEC/D3 (▲), and HBMVEC (▼). Cells were exposed to the β-isomer of PGEs (5 mM β-PGME, 1 mM β-PGEE, 0.1 mM β-PGBE, 0.12 mM β-PGPhE) for 24 h. Conversion of the β-PGEs to their corresponding β-metabolites (2-MPA, 2-EPA, 2-BPA, 2-PhPA), respectively, was determined by HPLC-MS/MS. Data are expressed as amount of β-metabolite formed per incubational protein content (pmol/µg). N = 3–5 independent biological repeats with 2 technical replicates (HepaRG), N = 3 independent biological repeats with 2–3 technical replicates (hCMEC/D3, HBMVEC), and N = 2–3 independent biological repeats with 2 technical replicates (pHH, N = 2, HUM201221 and HUM183121 each, N = 3 including HUM180871). Bar graphs represent means ± SD. **(B)** β-metabolite formation-time profiles in BrainSpheres. Cells were exposed to β-PGEs (20 mM β-PGME, β-PGEE) for 6 h. Conversion of the β-PGEs into their corresponding β-metabolites (2-MPA, 2-EPA), respectively, was determined by HPLC-MS/MS. Data are expressed as amount of β-metabolite formed per incubational protein content (pmol/µg). N = 3 independent biological repeats with 3 technical replicates. Bar graphs represent means ± SD, statistical analysis was based on Student's unpaired *t*-test: *, $p \leq 0.05$.

**Table 8**
Results for the assessment of β-metabolites formation in the different cell systems for the liver and CNS.

| | 3D HepaRG | | 3D primary human hepatocytes | | hCMEC/D3 | | HBMVEC | | | 3D BrainSpheres | |
|---|---|---|---|---|---|---|---|---|---|---|---|
| | (pmol/µg) | Ratio | (pmol/µg) | Ratio | (pmol/µg) | Ratio | (pmol/µg) | Ratio | | (pmol/µg) | Ratio |
| 5 mM β-PGME → 2-MPA 6 h | 8.55 ± 0.72 | **1.00** ± 0.08 | 15.6 | 1.82 | 2.79 ± 0.17 | 0.33 ± 0.02 | 1.68 ± 0.56 | 0.20 ± 0.07 | 20 mM β-PGME → 2-MPA 6 h | 4.30 ± 1.33 | ND |
| 5 mM β-PGME → 2-MPA 24 h | 15.3 ± 2.24 | **1.00** ± 0.15 | 15.7 ± 3.35 | 1.03 ± 0.22 | 2.84 ± 0.25 | 0.19 ± 0.02 | 1.57 ± 0.40 | 0.10 ± 0.03 | 20 mM β-PGME → 2-MPA 24 h | ND | ND |
| 1 mM β-PGEE → 2-EPA 6 h | 10.5 ± 5.14 | **1.00** ± 0.49 | 12.9 ± 4.46 | 1.23 ± 0.43 | 1.67 ± 0.24 | 0.16 ± 0.02 | 1.35 ± 0.11 | 0.13 ± 0.01 | 20 mM β-PGEE → 2-EPA 6 h | 12.9 ± 3.90 | ND |
| 1 mM β-PGEE → 2-EPA 24 h | 8.80 ± 4.87 | **1.00** ± 0.55 | 13.6 ± 4.07 | 1.55 ± 0.46 | 1.59 ± 0.20 | 0.18 ± 0.02 | 1.34 ± 0.17 | 0.15 ± 0.02 | 20 mM β-PGEE → 2-EPA 24 h | ND | ND |
| 0.1 mM β-PGBE → 2-BPA 6 h | 5.00 ± 1.30 | **1.00** ± 0.26 | 5.07 | 1.01 | < LOD | ND | < LOD | ND | | | |
| 0.1 mM β-PGBE → 2-BPA 24 h | 7.29 ± 3.14 | **1.00** ± 0.43 | 4.59 ± 0.29 | 0.63 ± 0.04 | < LOD | ND | < LOD | ND | | | |
| 0.12 mM β-PGPhE → 2-PhPA 6 h | 11.3 ± 5.90 | **1.00** ± 0.52 | 15.4 ± 6.20 | 1.36 ± 0.55 | < LOD | ND | < LOD | ND | | | |
| 0.12 mM β-PGPhE → 2-PhPA 24 h | 8.35 ± 1.60 | **1.00** ± 0.19 | 19.9 ± 10.7 | 2.39 ± 1.28 | < LOD | ND | < LOD | ND | | | |

ND: not determined. Data expressed as the amount of β-metabolite formed per incubational protein content (pmol/µg) at 6 h and 24 h. Ratios are calculated relative to 3D HepaRG (ratio 1.0) that serve as the benchmark standard. The β-PGEs are ordered by increasing lipophilicity (based on logP) from top to bottom. Abbreviations: LOD: limit of detection; CNS: central nervous system.

et al., 2012). However, the determination of *in vitro* hepatic intrinsic clearance ($CL_{int}$) did not necessarily require a long-lasting *in vitro* model, as linear metabolite formation was observed within the first hour. Nevertheless, 3D HepaRG can be used for more complex studies, such as organ-on-chip systems, over longer incubation periods. Although, a higher *in vitro* $CL_{int}$ was obtained with S9 than with 3D HepaRG, this was consistent with reported findings using liver cell fractions and hepatocytes (Bowman and Benet, 2016; Wood et al., 2017) and might be explained by limited enzyme accessibility (cell membrane), reduced co-factor availability, non-specific binding (e.g. serum), or reduced viability and functionality for the cell systems.

Applied to the β-PGEs, calculations based on the Michaelis-Menten-

kinetics (MMK) based on S9 biotransformation revealed a trend for an increasing *in vitro* $CL_{int}$ and extrapolated hepatic organ clearance ($CL_h$) with higher carbon chain length of the β-PGEs. This finding aligns with previous studies on the MMK of ethylene glycol ethers (EGEs) (Louisse et al., 2010) and with a study on substrate specificity of ADH (Aasmoe and Aarbakke, 1999). On the contrary, no specific pattern emerged for the measured *in vitro* $CL_{int}$ derived from 3D HepaRG. It remains unclear whether this outcome is due to the more complex incubation setup and the use of a 3D *in vitro* system, in which the substrates might require more time to reach the cells (lower *in vitro* bioavailability). To assess the predictive accuracy of the calculated ($V_{max}/K_m$) or measured clearance values, comparisons with available *in vivo* data would be necessary. Also, *in silico* predictions using structure-based analysis could provide further insights into enzyme-substrate affinities.

Based on the obtained calculated hepatic clearances, we propose to classify the selected β-PGEs as low to medium clearance compounds (Hultman et al., 2016; Kratochwil et al., 2017; Słoczyńska et al., 2019). Consequently, we speculate that the β-PGEs would not undergo rapid metabolism in the liver but would remain in the systemic circulation and thus reach the CNS. This is particularly relevant in the context of the observed interactions of PGEs with the CNS (high BBB permeance and active biotransformation). The low clearance would also influence the toxicokinetic and the related hazard of PGEs that are themselves highly toxic, as was the case for PGPhE and β-PGPhE on liver and BBB-tissue.

In order to ultimately estimate the neurotoxic potential of the selected PGEs, the determined NOAEC (no-observed-adverse-effect concentration) derived from *in vitro* experiments using BrainSpheres will be incorporated into a toxicokinetic model to predict safe air concentrations for humans *via* reverse dosimetry (Hopf et al., 2024). As there existed limited data for the selected PGEs on the hepatic kinetics of β-metabolite formation *in vitro* and in human, estimating PGE and β-metabolite brain exposures remained challenging in the past (ECETOC, 2005a, 2005b). With our results, we provide new input data on these PGEs using new approach methodologies, such as two *in vitro* liver models (3D HepaRG, S9), as an alternative to long-lasting and expensive animal experiments (Bal-Price et al., 2018).

With regards to cytotoxicity and similarly to reported findings with perfluorinated carboxylic acids on cancer cell lines (Mulkiewicz et al., 2007), we observed increasing toxic potential of the PGEs on HepaRG and hCMEC/D3 with higher chain length and lipophilicity (logP). The $EC_{50}$ values for the PGEs obtained on HepaRG and hCMEC/D3 were consistently lower (up to 171-fold) in comparison to EGME, which is banned due to its known toxic effects on testis, thymus, fetus, bone marrow, amongst others (Bagchi and Waxman, 2008; Beattie and Brabec, 1986). Besides, the cytotoxicity of ethanol, which is known for its neurological disturbances (Pervin and Stephen, 2021), was much lower than for the glycol ethers. These findings, in addition to the observed high sensitivity to β-metabolite exposure of the hCMEC/D3, support the conclusion that neurotoxicity in humans cannot be excluded and underline the importance of investigating the neurotoxic potential of the PGEs and their β-metabolites.

The ultimate mechanism of toxicity cannot be determined at this time. As the BBB integrity was not disturbed after two-days PGE exposure at predicted total extravascular concentration for the brain, we deem acute indirect neurotoxic effects due to an opening of the BBB unlikely. However, the applied concentration was based on toxicokinetic predictions for propylene glycol methyl ether (PGME) (Reale et al., 2023) and estimations on the extravascular brain concentration for each PGE would be needed. Furthermore, we observed lower $EC_{50}$ values for the β-PGEs than the PGE mixtures, consisting of $< 0.5$ % β-isomer. We cannot exclude that the higher toxicity was due to the higher extent of potentially toxic β-metabolites formed during the incubation period for the β-PGEs. However, the β-metabolites did not consistently show higher cytotoxicity than their parent solvents. Therefore, we speculate that both PGE- and β-PGE-induced toxicity were more likely due to the disruption of the cell membrane at high concentrations (Flores et al., 1994) rather than primarily through the formation of β-metabolite.

## 5. Conclusion

In conclusion, our results provide clear evidence for propylene glycol ether (PGE) metabolism *via* alcohol and aldehyde dehydrogenase in the central nervous system (CNS). This is of high relevance as neurotoxicity by PGEs may be enhanced through the active formation of alkoxy propionic acids (β-metabolites) at the target site. Therefore, we recommend considering extra-hepatic metabolism by the CNS when evaluating the neurotoxic effects of PGEs using New Approach Methods (NAMs) followed by quantitative *in-vitro* to *in-vivo* extrapolation for hazard assessment.

In addition, the hepatic clearance data generated in this study will serve as crucial input parameter for future toxicokinetic models, aimed at predicting the neurotoxic potential of PGEs. Furthermore, our work supports the use of the advanced 3D HepaRG model for studies that focus on the adverse effects of compound metabolites formed *via* the ADH/ALDH pathway, also applicable in more complex multi-organ studies or chronic exposure scenarios.

Finally, our findings may help to rank the PGEs based on their chemical properties (e.g. carbonic chain length and lipophilicity) in relation to their cytotoxicity and *in vitro* hepatic clearance.

## Funding statement

This study was funded by the Swiss Center for Applied Human Toxicology (SCAHT), Grant no. SCAHT-GL 21-10.

## CRediT authorship contribution statement

**Werner Sophie:** Writing – review & editing, Writing – original draft, Visualization, Validation, Resources, Project administration, Methodology, Investigation, Formal analysis, Conceptualization. **Zurich Marie-Gabrielle:** Writing – review & editing, Validation, Supervision, Resources, Funding acquisition. **Pamies David:** Writing – review & editing, Validation, Resources, Investigation, Formal analysis. **SUTER - DICK LAURA:** Writing – review & editing, Validation, Supervision, Resources, Project administration, Methodology, Funding acquisition, Conceptualization.

## Conflict of Interest

The authors declare no conflict of interest. The funders had no role in the design of the study; in the collection, analyses, or interpretation of data; in the writing of the manuscript, or in the decision to publish the results. David Pamies is named inventor on a patent by Johns Hopkins University on the production of mini-brains (also called BrainSpheres), which is licensed to AxoSim, New Orleans, LA, USA.

## Declaration of Competing Interest

The authors declare the following financial interests/personal relationships which may be considered as potential competing interests: Laura Suter-Dick reports financial support was provided by Swiss Center for Applied Human Toxicology (SCAHT). Sophie Werner reports financial support was provided by Swiss Center for Applied Human Toxicology (SCAHT). David Pamies reports financial support was provided by Swiss Center for Applied Human Toxicology (SCAHT). Marie-Gabrielle Zurich reports financial support was provided by Swiss Center for Applied Human Toxicology (SCAHT). David Pamies has patent mini-brains (also called BrainSpheres) licensed to AxoSim, New Orleans, LA, USA. If there are other authors, they declare that they have no known competing financial interests or personal relationships that could have appeared to influence the work reported in this paper.

## Acknowledgment

We would like to thank Timm Hettich and André Büttler at the FHNW for their valuable assistance in the development of the analytical methods and Jörg Huwyler for his scientific advice. We thank the Swiss Centre for Applied Human Toxicity (SCAHT), as well as our home institution FHNW for funding the research.

## Appendix A. Supporting information

Supplementary data associated with this article can be found in the online version at doi:10.1016/j.tox.2025.154081.

## Data availability

Data will be made available on request.

## References

Aasmoe, L., Aarbakke, J., 1999. Sex-dependent induction of alcohol dehydrogenase activity in rats. Biochem. Pharmacol. 57 (9), 1067–1072. https://doi.org/10.1016/S0006-2952(99)00003-9.

Aasmoe, L., Winberg, J.O., Aarbakke, J., 1998. The role of liver alcohol dehydrogenase isoenzymes in the oxidation of glycolethers in male and female rats. Toxicol. Appl. Pharmacol. 150 (1), 86–90. https://doi.org/10.1006/taap.1998.8410.

Bagchi, G., Waxman, D.J., 2008. Toxicity of ethylene glycol monomethyl ether: impact on testicular gene expression. Int. J. Androl. 31 (2), 269–274. https://doi.org/10.1111/j.1365-2605.2007.00846.x.

Bagchi, S., Chhibber, T., Lahooti, B., Verma, A., Borse, V., Jayant, R.D., 2019. In-vitro blood-brain barrier models for drug screening and permeation studies: an overview. Drug Des. Dev. Ther. 13, 3591–3605. https://doi.org/10.2147/DDDT.S218708.

Bal-Price, A., Pistollato, F., Sachana, M., Bopp, S.K., Munn, S., Worth, A., 2018. Strategies to improve the regulatory assessment of developmental neurotoxicity (DNT) using in vitro methods. Toxicol. Appl. Pharmacol. 354 (December 2017), 7–18. https://doi.org/10.1016/j.taap.2018.02.008.

Barter, Z., Bayliss, M., Beaune, P., Boobis, A., Carlile, D., Edwards, R., Brian Houston, J., Lake, B., Lipscomb, J., Pelkonen, O., Tucke, G., Rostami-Hodjegan, A., 2006. Scaling factors for the extrapolation of in vivo metabolic drug clearance from in vitro data: reaching a consensus on values of human micro-somal protein and hepatocellularity per gram of liver. Curr. Drug Metab. 8 (1), 33–45. https://doi.org/10.2174/138920007779315053.

Beattie, P.J., Brabec, M.J., 1986. Methoxyacetic acid and ethoxyacetic acid inhibit mitochondrial function in vitro. J. Biochem. Toxicol. 1 (3), 61–70. https://doi.org/10.1002/jbt.2570010307.

Bendels, S., Kansy, M., Wagner, B., Huwyler, J., 2008. In silico prediction of brain and CSF permeation of small molecules using PLS regression models. Eur. J. Med. Chem. 43 (8), 1581–1592. https://doi.org/10.1016/j.ejmech.2007.11.011.

Benet, L.Z., Zia-Amirhosseini, P., 1995. Basic principles of pharmacokinetics. Toxicol. Pathol. 23 (2), 115–123. https://doi.org/10.1177/019262339502300203.

Berezhkovskiy, L.M., 2004. Volume of distribution at steady state for a linear pharmacokinetic system with peripheral elimination. J. Pharm. Sci. 93 (6), 1628–1640. https://doi.org/10.1002/jps.20073.

Biemans, E.A.L.M., Jäkel, L., de Waal, R.M.W., Kuiperij, H.B., Verbeek, M.M., 2017. Limitations of the hCMEC/D3 cell line as a model for Aβ clearance by the human blood-brain barrier. J. Neurosci. Res. 95 (7), 1513–1522. https://doi.org/10.1002/jnr.23964.

Bonn, B., Svanberg, P., Janefeldt, A., Hultman, I., Grime, K., 2016. Determination of human hepatocyte intrinsic clearance for slowly metabolized compounds: comparison of a primary hepatocyte/stromal cell co-culture with plated primary hepatocytes and hepaRG. Drug Metab. Dispos. 44 (4), 527–533. https://doi.org/10.1124/dmd.115.067769.

Bowman, C.M., Benet, L.Z., 2016. Hepatic clearance predictions from in vitro-in vivo extrapolation and the biopharmaceutics drug disposition classification system. Drug Metab. Dispos. 44 (11), 1731–1735. https://doi.org/10.1124/dmd.116.071514.

Brown, R.C., Lockwood, A.H., Sonawane, B.R., 2005. Neurodegenerative diseases: an overview of environmental risk factors. Environ. Health Perspect. 113 (9), 1250–1256. https://doi.org/10.1289/ehp.7567.

Carney, E.W., Pottenger, L.H., Johnson, K.A., Liberacki, A.B., Tornesi, B., Dryzga, M.D., Hansen, S.C., Breslin, W.J., 2003. Significance of 2-methoxypropionic acid formed from β-propylene glycol monomethyl ether: integration of pharmacokinetic and developmental toxicity assessments in rabbits. Toxicol. Sci. 71 (2), 217–228. https://doi.org/10.1093/toxsci/71.2.217.

Choublier, N., Müller, Y., Gomez Baisac, L., Laedermann, J., de Rham, C., Declèves, X., Roux, A., 2021. Blood–brain barrier dynamic device with uniform shear stress distribution for microscopy and permeability measurements. Appl. Sci. 11 (12). https://doi.org/10.3390/app11125584.

Crabb, D.W., Matsumoto, M., Chang, D., You, M., 2004. Overview of the role of alcohol dehydrogenase and aldehyde dehydrogenase and their variants in the genesis of alcohol-related pathology. Proc. Nutr. Soc. 63 (1), 49–63. https://doi.org/10.1079/pns2003327.

Davies, B., Morris, T., 1993. Physiological parameters in laboratory animals and humans. Pharm. Res. 10 (7), 1093–1095.

ECETOC, 2005a. The toxicology of glycol ethers and its relevance to man (fourth edition). Volume I. Technical report no. 95. Tech. Rep., vol. I(no. 95), pp. 159–62. ⟨http://www.ecetoc.org/wp-content/uploads/2014/08/ECETOC-TR-095-Vol-I.pdf%0A⟩.

ECETOC, 2005b. The Toxicology of Glycol Ethers and Its Relevance to Man (Fourth Edition). Volume II – substance profiles. Tech. Rep., vol. II(no. 95), pp. 159–62. ⟨http://www.ecetoc.org/wp-content/uploads/2014/08/ECETOC-TR-095-Vol-II.pdf⟩.

Edenberg, H.J., 2007. The genetics of alcohol metabolism: role of alcohol dehydrogenase and aldehyde dehydrogenase variants. Alcohol Res. Health 30 (1), 5–13.

Eigenmann, D.E., Xue, G., Kim, K.S., Moses, A.V., Hamburger, M., Oufir, M., 2013. Comparative study of four immortalized human brain capillary endothelial cell lines, hCMEC/D3, hBMEC, TY10, and BB19, and optimization of culture conditions, for an in vitro blood-brain barrier model for drug permeability studies. Fluids Barriers CNS 10 (1). https://doi.org/10.1186/2045-8118-10-33.

Evelina, S., Zhong, W., Fagerberg, L., Karlsson, M., Mitsios, N., Adori, C., Oksvold, P., Edfors, F., Limiszewska, A., Hikmet, F., Huang, J., Du, Y., Lin, L., Dong, Z., Yang, L., Liu, X., Jiang, H., Xu, X., Wang, J., Mulder, J., et al., 2020. An atlas of the protein-coding genes in the human, pig, and mouse brain. Science 367 (6482). https://doi.org/10.1126/science.aay5947.

Chen, Feng, 2020. Broad distribution of hepatocyte proliferation in liver homeostasis and regeneration. Cell Stem Cell 26 (1), 27–33. https://doi.org/10.1016/j.stem.2019.11.001.

Flores, M.V., Voget, C.E., Ertola, R.J.J., 1994. Permeabilization of yeast cells (Kluyveromyces lactis) with organic solvents. Enzym. Microb. Technol. 16 (4), 340–346. https://doi.org/10.1016/0141-0229(94)90177-5.

Galter, D., Carmine, A., Buervenich, S., Duester, G., Olson, L., 2003. Distribution of class I, III and IV alcohol dehydrogenase mRNAS in the adult rat, mouse and human brain. Eur. J. Biochem. 270 (6), 1316–1326. https://doi.org/10.1046/j.1432-1033.2003.03502.x.

Geldenhuys, W.J., Mohammad, A.S., Adkins, C.E., Lockman, P.R., 2015. Molecular determinants of blood-brain barrier permeation. Ther. Deliv. 6 (8), 961–971. https://doi.org/10.4155/tde.15.32.

Hallifax, D., Houston, J.B., 2006. Binding of drugs to hepatic microsomes: comment and assessment of current prediction methodology with recommendation for improvement. Drug Metab. Dispos. 34 (4), 727. https://doi.org/10.1124/dmd.105.009142.

Haorah, J., Knipe, B., Leibhart, J., Ghorpade, A., Persidsky, Y., 2005. Alcohol-induced oxidative stress in brain endothelial cells causes blood-brain barrier dysfunction. J. Leukoc. Biol. 78 (6), 1223–1232. https://doi.org/10.1189/jlb.0605340.

Heit, C., Dong, H., Chen, Y., Thompson, D.C., Deitrich, R.A., Vasiliou, V.K., 2013. The role of CYP2E1 in alcohol metabolism and sensitivity in the central nervous system. Subcell. Biochem. 67 (Brust 2010), 235–247. https://doi.org/10.1007/978-94-007-5881-0_8.

Hogberg, H.T., Bressler, J., Christian, K.M., Harris, G., Makri, G., O'Driscoll, C., Pamies, D., Smirnova, L., Wen, Z., Hartung, T., 2013. Toward a 3D model of human brain development for studying gene/environment interactions. Stem Cell Res. Ther. 4 (.1), 1–7. https://doi.org/10.1186/scrt365.

Hopf, N.B., Suter-Dick, L., Huwyler, J., Borgatta, M., Hegg, L., Pamies, D., Paschoud, H., Puligilla, R.D., Reale, E., Werner, S., Zurich, M.-G., 2024. Novel strategy to assess the neurotoxicity of organic solvents such as glycol ethers: protocol for combining in vitro and in silico methods with human-controlled exposure experiments. JMIR Res. Protoc. 13, e50300. https://doi.org/10.2196/50300.

Houston, J., Galetin, A., 2008. Methods for predicting in vivo pharmacokinetics using data from in vitro assays. Curr. Drug Metab. 9 (9), 940–951. https://doi.org/10.2174/138920008786485164.

Hultman, I., Vedin, C., Abrahamsson, A., Winiwarter, S., Darnell, M., 2016. Use of HμREL human coculture system for prediction of intrinsic clearance and metabolite formation for slowly metabolized compounds. Mol. Pharm. 13 (8), 2796–2807. https://doi.org/10.1021/acs.molpharmaceut.6b00396.

Ingelman-Sundberg, M., Lauschke, V.M., 2021. 3D human liver spheroids for translational pharmacology and toxicology, 130 (S1), 5–15. https://doi.org/10.1111/bcpt.13587.

Jiang, Y., Zhang, T., Kusumanchi, P., Han, S., Zhihong, Y., Liangpunsakul, S., 2020. Alcohol metabolizing enzymes, microsomal ethanol oxidizing system, cytochrome P450 2E1, catalase, and aldehyde dehydrogenase in alcohol-associated liver disease. Biomedicines 8 (50), 1–16.

Jones, H.M., Rowland-Yeo, K., 2013. Basic concepts in physiologically based pharmacokinetic modeling in drug discovery and development. CPT: Pharmacomet. Syst. Pharmacol. 2 (8), 1–12. https://doi.org/10.1038/psp.2013.41.

Kanebratt, K.P., Janefeldt, A., Vilén, L., Vildhede, A., Samuelsson, K., Milton, L., Björkbom, A., Persson, M., Leandersson, C., Andersson, T.B., Hilgendorf, C., 2021. Primary human hepatocyte spheroid model as a 3D in vitro platform for metabolism studies. J. Pharm. Sci. 110 (1), 422–431. https://doi.org/10.1016/j.xphs.2020.10.043.

Kilford, P.J., Gertz, M., Houston, J.B., Galetin, A., 2008. Hepatocellular binding of drugs: correction for unbound fraction in hepatocyte incubations using microsomal binding or drug lipophilicity data. Drug Metab. Dispos. 36 (7), 1194–1197. https://doi.org/10.1124/dmd.108.020834.

Kim, J., Shin, S.A., Lee, C.S., Chung, H.J., 2024. An improved in vitro blood-brain barrier model for the evaluation of drug permeability using transwell with shear stress. Pharmaceutics 16 (1). https://doi.org/10.3390/pharmaceutics16010048.

Kratochwil, N.A., Meille, C., Fowler, S., Klammers, F., Ekiciler, A., Molitor, B., Simon, S., Walter, I., McGinnis, C., Walther, J., Leonard, B., Triyatni, M., Javanbakht, H.,

Funk, C., Schuler, F., Lavé, T., Parrott, N.J., 2017. Metabolic profiling of human long-term liver models and hepatic clearance predictions from in vitro data using nonlinear mixed-effects modeling. AAPS J. 19 (2), 534–550. https://doi.org/10.1208/s12248-016-0019-7.

Landry, T.D., Yano, B.L., 1984. Dipropylene glycol monomethyl ether: a 13-week inhalation toxicity study in rats and rabbits. Toxicol. Sci. 4 (4), 612–617. https://doi.org/10.1093/toxsci/4.4.612.

Laniewska-Dunaj, M., Jelski, W., Orywal, K., Kochanowicz, J., Rutkowski, R., Szmitkowski, M., 2013. The activity of class I, II, III and IV of alcohol dehydrogenase (ADH) isoenzymes and aldehyde dehydrogenase (ALDH) in brain cancer. Neurochem. Res. 38 (7), 1517–1521. https://doi.org/10.1007/s11064-013-1053-9.

Lobell, M., Sivarajah, V., 2003. In silico prediction of aqueous solubility, human plasma protein binding and volume of distribution of compounds from calculated pKa and AlogP98 values. Mol. Divers. 7 (1), 69–87. https://doi.org/10.1023/B:MODI.0000006562.93049.36.

Louisse, J., de Jong, E., van de Sandt, J.J.M., Blaauboer, B.J., Woutersen, R.A., Piersma, A.H., Rietjens, I.M.C.M., Verwei, M., 2010. The use of in vitro toxicity data and physiologically based kinetic modeling to predict dose-response curves for in vivo developmental toxicity of glycol ethers in rat and man. Toxicol. Sci. 118 (2), 470–484. https://doi.org/10.1093/toxsci/kfq270.

Lübberstedt, M., Müller-Vieira, U., Mayer, M., Biemel, K.M., Knöspel, F., Knobeloch, D., Nüssler, A.K., Gerlach, J.C., Zeilinger, K., 2011. HepaRG human hepatic cell line utility as a surrogate for primary human hepatocytes in drug metabolism assessment in vitro. J. Pharmacol. Toxicol. Methods 63 (1), 59–68. https://doi.org/10.1016/j.vascn.2010.04.013.

Mandon, M., Huet, S., Dubreil, E., Fessard, V., Le Hégarat, L., 2019. Three-dimensional HepaRG spheroids as a liver model to study human genotoxicity in vitro with the single cell gel electrophoresis assay. Sci. Rep. 9 (1), 1–9. https://doi.org/10.1038/s41598-019-47114-7.

Martínez, S.E., Vaglenova, J., Sabrià, J., Carmen Martínez, M., Farrés, J., Parés, X., 2001. Distribution of alcohol dehydrogenase mRNA in the rat central nervous system: consequences for brain ethanol and retinoid metabolism. Eur. J. Biochem. 268 (19), 5045–5056. https://doi.org/10.1046/j.0014-2956.2001.02416.x.

Miller, R.R., Hermann, E.A., Langvardt, P.W., McKenna, M.J., Schwetz, B.A., 1983. Comparative metabolism and disposition of ethylene glycol monomethyl ether and propylene glycol monomethyl ether in male rats. Toxicol. Appl. Pharmacol. 67 (2), 229–237. https://doi.org/10.1016/0041-008X(83)90229-6.

Miller, R.R., Hermann, E.A., Young, J.T., 1984. Ethylene glycol monomethyl ether and propylene glycol monomethyl ether: metabolism, disposition, and subchronic inhalation toxicity studies. Environ. Health Perspect. 57, 233–239. https://doi.org/10.1289/ehp.8457233.

Miller, R.R., Hermann, E.A., Young, J.T., Calhoun, L.L., Kastl, P.E., 1984. Propylene glycol monomethyl ether acetate (PGMEA) metabolism, disposition, and short-term vapor inhalation toxicity studies. Toxicol. Appl. Pharmacol. 75 (3), 521–530. https://doi.org/10.1016/0041-008X(84)90188-1.

Moslen, M.T., Kaphalia, L., Balasubramanian, H., Yina, Y. mei, Au, W.W., 1995. Species differences in testicular and hepatic biotransformation of 2-methoxyethanol. Toxicology 96 (3), 217–224. https://doi.org/10.1016/0300-483X(94)02921-G.

Mukaka, M.M., 2012. Statistics corner: a guide to appropriate use of correlation coefficient in medical research. Malawi Med. J. 24 (3), 69–71.

Mulkiewicz, E., Jastorff, B., Składanowski, A.C., Kleszczyński, K., Stepnowski, P., 2007. Evaluation of the acute toxicity of perfluorinated carboxylic acids using eukaryotic cell lines, bacteria and enzymatic assays. Environ. Toxicol. Pharmacol. 23 (3), 279–285. https://doi.org/10.1016/j.etap.2006.11.002.

Musther, H., Harwood, M.D., Yang, J., Turner, D.B., Rostami-Hodjegan, A., Jamei, M., 2017. The constraints, construction, and verification of a strain-specific physiologically based pharmacokinetic rat model. J. Pharm. Sci. 106 (9), 2826–2838. https://doi.org/10.1016/j.xphs.2017.05.003.

Nunes, C., Proença, S., Ambrosini, G., Pamies, D., Thomas, A., Kramer, N.I., Zurich, M., 2023. Integrating distribution kinetics and toxicodynamics to assess repeat dose neurotoxicity in vitro using human BrainSpheres: a case study on amiodarone. vol. September, pp. 1–15. ⟨https://doi.org/10.3389/fphar.2023.1248882⟩.

Obach, R.S., Baxter, J.G., Liston, T.E., et al., 1997. The Prediction of Human Pharmacokinetic Parameters From Preclinical and In Vitro Metabolism Data. J. Pharmacol. Exp. Ther. 283 (1), 46–58.

Pamies, D., Chesnut, M., Smirnova, L., Mutallimov, A., Maillard, V., Repond, C., Hartung, T., Zurich, M.-G., Hogberg, H., 2021. Human 3D iPSC-derived brain model to study chemical-induced myelin disruption. Int. J. Mol. Sci. 22 (9473), 1–20. https://doi.org/10.3390/ijms22179473.

Pamies, David, Barreras, P., Block, K., Makri, G., Kumar, A., Wiersma, D., Smirnova, L., Zhang, C., Bressler, J., Christian, K.M., Harris, G., Ming, G.L., Berlinicke, C.J., Kyro, K., Song, H., Pardo, C.A., Hartung, T., Hogberg, H.T., 2017. A human brain microphysiological system derived from induced pluripotent stem cells to study neurological diseases and toxicity. Altex 34 (3), 362–376. https://doi.org/10.14573/altex.1609122.

Pamies, David, Block, K., Lau, P., Gribaldo, L., Pardo, C.A., Barreras, P., Smirnova, L., Wiersma, D., Zhao, L., Harris, G., Hartung, T., Hogberg, H.T., 2018. Rotenone exerts developmental neurotoxicity in a human brain spheroid model. Toxicol. Appl. Pharmacol. 354 (January), 101–114. https://doi.org/10.1016/j.taap.2018.02.003.

Pang, K.S., Rowland, M., 1977. Hepatic clearance of drugs. I. Theoretical considerations of a "well-stirred" model and a "parallel tube" model. Influence of hepatic blood flow, plasma and blood cell binding, and the hepatocellular enzymatic activity on hepatic drug clearance. J. Pharmacokinet. Biopharm. 5 (6), 625–653. https://doi.org/10.1007/BF01059688.

Pearce, N., Kromhout, H., 2014. Neurodegenerative disease: the next occupational disease epidemic? Occup. Environ. Med. 71 (9), 594–595. https://doi.org/10.1136/oemed-2013-101943.

Pervin, Z., Stephen, J.M., 2021. Effect of alcohol on the central nervous system to develop neurological disorder: pathophysiological and lifestyle modulation can be potential therapeutic options for alcohol-induced neurotoxication. AIMS Neurosci. 8 (3), 390–413. https://doi.org/10.3934/NEUROSCIENCE.2021021.

Poller, B., Gutmann, H., Krähenbühl, S., Weksler, B., Romero, I., Couraud, P.O., Tuffin, G., Drewe, J., Huwyler, J., 2008. The human brain endothelial cell line hCMEC/D3 as a human blood-brain barrier model for drug transport studies. J. Neurochem. 107 (5), 1358–1368. https://doi.org/10.1111/j.1471-4159.2008.05730.x.

Price, A., Pistollato, F., Munn, S., Bopp, S., Worth, A., 2018. Strategic aims for improving the regulatory assessment of developmental neurotoxicity (DNT) using non-animal methods. JRC Tech. Rep. https://doi.org/10.2760/03355.

Quertemont, E., 2004. Genetic polymorphism in ethanol metabolism: acetaldehyde contribution to alcohol abuse and alcoholism. Mol. Psychiatry 9 (6), 570–581. https://doi.org/10.1038/sj.mp.4001497.

Ramaiahgari, S.C., Waidyanatha, S., Dixon, D., DeVito, M.J., Paules, R.S., Ferguson, S.S., 2017. Three-dimensional (3D) HepaRG spheroid model with physiologically relevant xenobiotic metabolism competence and hepatocyte functionality for liver toxicity screening. Toxicol. Sci. 159 (1), 124–136. https://doi.org/10.1093/toxsci/kfx122.

Reale, E., Sandstrom, J., Culot, M., Hechon, J., Wellens, S., Heymans, M., Tschudi-Monnet, F., Vernez, D., Hopf, N.B., 2023. Predicting human neurotoxicity of propylene glycol methyl ether (PGME) by implementing in vitro neurotoxicity results into toxicokinetic modelling. Sci. Total Environ. 886 (February), 163767. https://doi.org/10.1016/j.scitotenv.2023.163767.

Riley, R.J., McGinnity, D.F., Austin, R.P., 2005. A unified model for predicting human hepatic, metabolic clearance from in vitro intrinsic clearance data in hepatocytes and microsomes. Drug Metab. Dispos. 33 (9), 1304–1311. https://doi.org/10.1124/dmd.105.004259.

Shah, R., Babar, A., Patel, A., Dortonne, R., Jordan, J., 2020. Metoprolol-associated central nervous system complications. Cureus 12 (5). https://doi.org/10.7759/cureus.8236.

Słoczyńska, K., Gunia-Krzyzak, A., Koczurkiewicz, P., Wójcik-Pszczoła, K., Zelaszczyk, D., Popiół, J., Pękala, E., 2019. Metabolic stability and its role in the discovery of new chemical entities. Acta Pharm. 69 (3), 345–361. https://doi.org/10.2478/acph-2019-0024.

Smith, C.M., Nolan, C.K., Edwards, M.A., Hatfield, J.B., Stewart, T.W., Ferguson, S.S., Lecluyse, E.L., Sahi, J., 2012. A comprehensive evaluation of metabolic activity and intrinsic clearance in suspensions and monolayer cultures of cryopreserved primary human hepatocytes. J. Pharm. Sci. 101 (10), 3989–4002. https://doi.org/10.1002/jps.23262.

Sodhi, J.K., Benet, L.Z., 2021. Successful and unsuccessful prediction of human hepatic clearance for lead optimization. J. Med. Chem. 64 (7), 3546–3559. https://doi.org/10.1021/acs.jmedchem.0c01930.

Suenderhauf, C., Hammann, F., Huwyler, J., 2012a. Computational prediction of blood-brain barrier permeability using decision tree induction. Molecules 17 (9), 10429–10445. https://doi.org/10.3390/molecules170910429.

Suenderhauf, C., Hammann, F., Huwyler, J., 2012b. Computational prediction of blood-brain barrier permeability using decision tree induction. Molecules 17 (9), 10429–10445. https://doi.org/10.3390/molecules170910429.

Tsang, H.Y., Lo, P.H.Y., Kenneth, K.H.L., 2021. Generation of liver organoids from human induced pluripotent stem cells as liver fibrosis and steatosis models. Front. Neurosci. 14 (1), 1–13. https://doi.org/10.1101/2021.06.29.450347.

Wang, W., Wang, C., Xu, H., Gao, Y., 2020. Aldehyde dehydrogenase, liver disease and cancer. Int. J. Biol. Sci. 16 (6), 921–934. https://doi.org/10.7150/ijbs.42300.

Wang, Y., He, W., 2018. Endogenous mitochondrial aldehyde dehydrogenase-2 as an antioxidant in liver. In: The Liver: Oxidative Stress and Dietary Antioxidants. Elsevier Inc. https://doi.org/10.1016/B978-0-12-803951-9.00021-5.

Waring, M.J., 2009. Defining optimum lipophilicity and molecular weight ranges for drug candidates-Molecular weight dependent lower log D limits based on permeability. Bioorg. Med. Chem. Lett. 19 (10), 2844–2851. https://doi.org/10.1016/j.bmcl.2009.03.109.

Wei, J., Dai, Y., Wen, W., Li, J., Ye, L.L., Xu, S., Duan, D.D., 2021. Blood-brain barrier integrity is the primary target of alcohol abuse. Chem.-Biol. Interact. 337 (December 2020). https://doi.org/10.1016/j.cbi.2021.109400.

Weksler, B., Romero, I.A., Couraud, P.O., 2013. The hCMEC/D3 cell line as a model of the human blood brain barrier. Fluids Barriers CNS 10 (1), 1–10. https://doi.org/10.1186/2045-8118-10-16.

Wen, Z., Nguyen, H.N., Guo, Z., Lalli, M.A., Wang, X., Su, Y., Kim, N., Yoon, K., Shin, J., Zhang, C., Nauen, D., Yu, H., Guzman, E., Chiang, C., Kaibuchi, K., Zou, J., Christian, K.M., Cheng, L., Ross, C.A., Barbara, S., et al., 2015. Synaptic dysregulation in a human iPS cell model of mental disorders. Nature 515 (7527), 414–418. https://doi.org/10.1038/nature13716.Synaptic.

Werner, S., Hegg, L., Hopf, N.B., Borgatta, M., Suter-Dick, L., 2024. In vitro hepatic metabolism input parameters support toxicokinetic simulations for the formation of methoxy propionic acid from β-isomer propylene glycol methyl ether. Pharmacol. Biochem. Behav. 12 (6), 1–21. https://doi.org/10.1002/prp2.70037.

Wood, F.L., Houston, J.B., Hallifax, D., 2017. Clearance prediction methodology needs fundamental improvement: trends common to rat and human hepatocytes/

microsomes and implications for experimental methodology. Drug Metab. Dispos. 45 (11), 1178–1188. https://doi.org/10.1124/dmd.117.077040.
Yang, H., Lou, C., Sun, L., Li, J., Cai, Y., Wang, Z., Li, W., Liu, G., Tang, Y., 2019. AdmetSAR 2.0: web-service for prediction and optimization of chemical ADMET properties. Bioinformatics 35 (6), 1067–1069. https://doi.org/10.1093/bioinformatics/bty707.
Zimatkin, S.M., Deitrich, R.A., 1997. Ethanol metabolism in the brain. Addict. Biol. 2 (4), 387–400. https://doi.org/10.1080/13556219772444.